# Chapter 1

# MICROSTRUCTURE AND MECHANICAL PROPERTIES OF TITANIUM ALLOYS

G. Lütjering *, J. C. Williams** and A. Gysler*

*Technical University Hamburg-Harburg, Hamburg, Germany
**General Electric Aircraft Engines, Cincinnati, OH, USA

## 1. Introduction

Titanium was first identified as a new and unknown metallic element by Gregor in England (1791), and was named Titanium several years later (1795) by Klapproth in Germany after the Titans of the Greek mythology. The production of high-puity titanium proved to be difficult, because of the strong tendency of this metal to react with oxygen and nitrogen. Therefore, it was not until the middle of the 20th century (1938-1940) that a commercially attractive process was developed by W.J. Kroll in Luxemburg. This process involves the reduction of titanium tetrachloride with magnesium in an inert-gas atmosphere. The resulting titanium is called "titanium sponge" because of the porous, spongy appearance. The commercial interest in titanium and its alloys was prompted by the relatively low density of this metal (between those of aluminum and iron) in combination with a high yield strength (especially in the 200-450°C range), and its excellent corrosion resistance. Therefore, titanium and its alloys are used primarily in two areas of applications: corrosion resistant areas, such as the chemical industry, and in areas where weight-savings and high strength are predominant, such as in aircraft and aerospace applications. This introductory section is not intended to give an in-depth overview on the basic properties of titanium, but only to briefly summarize some of the findings which are important with regard to the main subject of this chapter on microsturcture/property relationships of titanium alloys.

The existing literature on titanium alloys is well documented in the Proceedings of the International Conferences on Titanium, which were held with one exception every four years: 1968 in London [1], 1972 in Boston [2], 1976 in Moscow [3], 1980 in Kyoto [4], 1984 in Munich [5], 1988 in Cannnes [6], 1992 in San Diego [7] and 1995 in Birmingham [8], the next conference being 1999 in St. Petersburg.

### 1.1 Crystal Structure

Titanium undergoes an allotropic phase tranformation at 882.5 °C, changing from a closed-packed hexagonal crystal structure ($\alpha$ phase) below, to a body-centered cubic crystal structure ($\beta$ phase) above this temperature. The exact transformation temperature is strongly influenced by interstitial and substitutional elements, therefore depending on the purity of the metal. The hcp unit cell of the low temperature $\alpha$ phase is shown in

Figure 1a, together with the three most densely packed lattice planes and the lattice parameters at room temperature. The resulting ratio c/a = 1.587 for pure α-Ti is smaller than the ideal ratio for a hexagonal closed packed crystal structure with c/a = 1.633. The unit cell of the bcc β phase is illustrated in Figure 1b, exhibiting one variant of the most densly packed {110} lattice planes, and the lattice parameter of pure β-Ti at 900 °C.

The intrinsic anisotropic behavior of the hexagonal crystal structure of the α phase has important consequences for the elastic and plastic deformation behavior of titanium and its alloys, besides on numerous other physical properties. The variation of Young's modulus E of pure α-Ti single crystals at room temperature as a function of the angle γ between the c-axis of the unit cell and the stress axis is shown in Figure 2 [9], resulting in modulus variations between 145 GPa (stress axis || c-axis) and 100 GPa (stress axis ⊥ c-axis). Similar strong variations are also observed for single crystal shear modulus values G of 46 GPa and 34 GPa for shear stresses applied in (0002) and $\{10\bar{1}0\}$ planes, respectively, with the stress axis being parallel to $< 11\bar{2}0 >$. Although such differences are smaller in polycrystalline α-Ti and its alloys, there can be still pronounced varations for highly textured material (see Section 2).

The elastic moduli are decreasing almost linearly with increasing test temperature up to the transformation temperature. For polycrystalline α-Ti without texture the Young's modulus drops from about 110 GPa at RT to about 58 GPa just below the transus, while the shear modulus decreases from about 42 to 20 GPa in the same temperature interval [e.g. 10].

Since the β phase of pure Ti cannot be retained at RT, Young's modulus values are shown here for binary Ti-V solid solution alloys in Figure 3. The moduli of β-Ti increase with increasing solute content and their values are much lower as compared to those in α-Ti. In general, commercial β-Ti alloys exhibit E-moduli at RT in the range of 70 to 90 GPa, while α and α+β Ti-alloys show values which are always above 100 GPa [11].

### 1.2 Deformation Modes

The observed ductile behavior of α-Ti, also at low testing temperatures, results from the combined contribution of slip and twinning modes.

#### 1.2.1 Slip Modes

The various slip systems observed in α-Ti are summarized in Table 1 and corresponding slip planes and slip directions in the hcp unit cell are shown in Figure 4. The three slip systems in Table 1, which all have the same $\vec{a}$ type Burgers vector, together possess nominally 8 independent slip systems. However, this number reduces to only 4 systems since the changes of shape that can be produced by the combined slip systems 1+2 are exactly the same as those of the slip system 3. In no case is an extension parallel to the c-axis possible. Therefore, in order to satisfy the von Mises criterion, which requires at least five independent slip systems for a homogeneous plastic deformation of

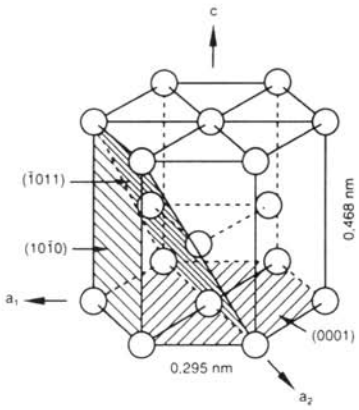


a) hcp α phase

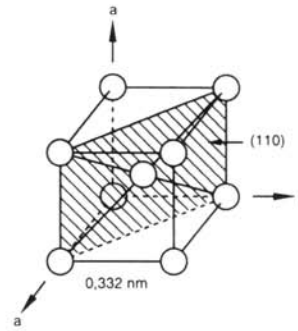


b) bcc β phase

Fig. 1: Unit cells of α and β phases.

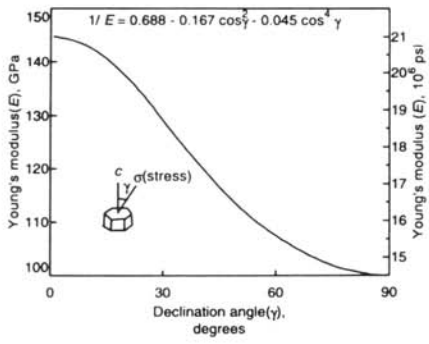


Fig. 2: Variation of Young's modulus (E) in α-Ti single crystals with declination angle (γ) [9].

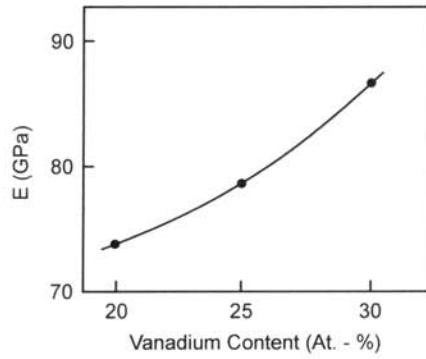


Fig. 3: Young's modulus (E) as a function of Vanadium content in β Ti-V solid solution alloys.

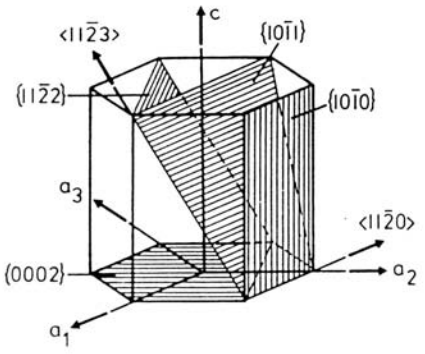


Fig. 4: Slip planes and slip directions in the hcp α phase.

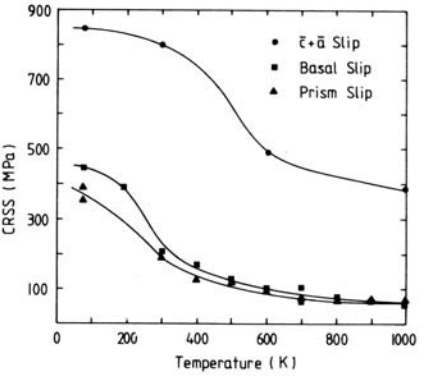


Fig. 5: CRSS for slip with $<\vec{a}>$ and $<\vec{c}+\vec{a}>$ Burgers vectors in solid solution Ti-6.6Al single crystals.

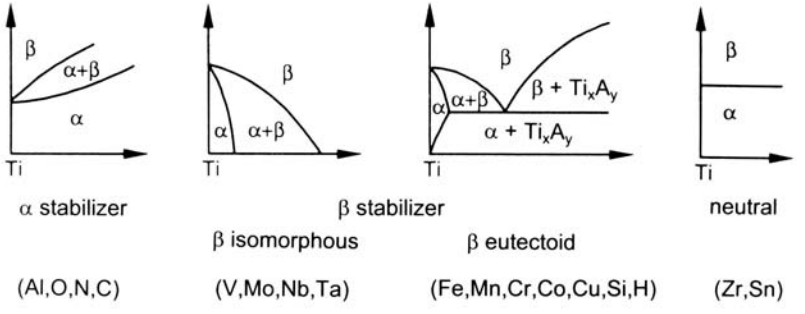


Fig. 6: Effect of alloying additions on equilibrium phase diagrams of Ti-alloys (schematically).

polycrystals, the operation of one of the slip systems $\{10\bar{1}1\}$ with a $\vec{c} + \vec{a}$ Burgers vector needs to be activated, which has been observed in a number of Ti-alloys [14, 15].

| Slip system | Burgers vector type | Slip direction | Slip plane | No. of slip systems total | independent |
|---|---|---|---|---|---|
| 1 | $\vec{a}$ | $<11\bar{2}0>$ | (0002) | 3 | 2 |
| 2 | $\vec{a}$ | $<11\bar{2}0>$ | $\{10\bar{1}0\}$ | 3 | 2 |
| 3 | $\vec{a}$ | $<11\bar{2}0>$ | $\{10\bar{1}1\}$ | 6 | 4 |
| 4 | $\vec{c} + \vec{a}$ | $<11\bar{2}3>$ | $\{10\bar{1}1\}$ | 12 | 5 |

Table 1: Slip systems in the hcp $\alpha$ phase [12, 13]

The predominant slip mode in α-Ti is $\{10\bar{1}0\} < 11\bar{2}0 >$, followed by $\{10\bar{1}1\}$ and (0002) both with an $\vec{a}$ type Burgers vector. The highest critical resolved shear stress (CRSS) is required for slip with $\vec{c} + \vec{a}$ Burgers vector. Absolute values of CRSS are strongly dependent on alloy content and on test temperature. An example of CRSS for three different slip systems in solid solution strengthened Ti-Al single crystals as a function of test temperature is shown in Figure 5 [16]. The very large difference in CRSS between slip with $\vec{a}$ and $\vec{c} + \vec{a}$ Burgers vectors as found in Ti-Al (Figure 5), was observed to be much smaller in a commercial α+β alloy [15].

The slip systems generally observed in β-Ti are {110}, {112} and {123}, all with the Burgers vector of < 111 >, as was found in binary Ti-Mo and Ti-V alloys [17].

### 1.2.2 Deformation Twinning

There are many twinning modes observed in titanium [12]. The crystallographic elements of two twin systems in α-Ti are listed in Table 2 as an example [12]. The $\{11\bar{2}1\}$ twins allow an extension along the c-axis, while the $\{11\bar{2}2\}$ twins permit a reduction. Therefore, twinning is very dependent on the sense of the applied stress, in

| Twinning plane (1st undeformed plane) ($K_1$) | Twinning shear direction ($\eta_1$) | Second undeformed plane ($K_2$) | Direction of intersection of plane of shear with $K_2$ ($\eta_2$) | Plane of shear perpendicular to $K_1$ and $K_2$ | Magnitude of twinning shear |
|---|---|---|---|---|---|
| $\{11\bar{2}1\}$ | $\{11\bar{2}6\}$ | (0001) | $<11\bar{2}0>$ | {1100} | 0.638 |
| $\{11\bar{2}2\}$ | $\{11\bar{2}3\}$ | $(11\bar{2}4)$ | $<22\bar{4}3>$ | {1100} | 0.225 |

Table 2: Twinning elements (examples) [12]

contrast to plastic deformation by dislocations. Increasing contents of solute atoms are suppressing twinning, such as oxygen or aluminum, therefore twinning as a deformation mode to allow a shape change parallel to the c-axis of α-Ti plays only a role in pure or commercial purity Ti with lower oxygen concentrations [14]. Twinning is also drastically reduced with decreasing grain sizes or phase dimensions [12].

### 1.3 Phase Diagrams

Alloying elements in Ti are classified into α or β stabilizers on the basis of their effects on the α/β transformation temperature or on their differing solubilities in the α or β phases. The substitutional element Al and the interstitials O, N and C are strong α-stabilizers and are increasing the transus temperature with increasing solute content, as shown in the schematic phase diagrams in Figure 6. The β-stabilizing elements are lowering the transus temperatur. Those are distinguished into β-isomorphous types (e.g. V, Mo, Nb, Ta) and β-entectoid types (e.g. Mn, Fe, Cr, Co, Ni. Cn, Si, H). Examples of these two diagram types are also shown in Figure 6. In addition, there exist other elements, for example Zr and Sn, which behave more or less neutral or are slightly decreasing the transus temperature (Figure 6). Actual equilibrium phase diagrams for all of these systems can be found in [18].

### 1.4 Phase Transformations

The transformation of the bcc β to the hcp α modification of high puity titanium by cooling through the transformation temperature occurs by a nucleation and shear type process. The crystallographic orientation relationship between α and β has first been studied for Zr by Burgers [19], and is therefore named Burgers-Relationship:

$$\{110\}_\beta \,//\, (0002)_\alpha$$

$$<111>_\beta \,//\, <11\bar{2}0>_\alpha$$

This relationship was confirmed later also for titanium [20]. According to this relationship a bcc crystal can therefore transform to 12 hexagonal variants, having different orientations with regard to the parent β crystal. This tranformation can occur in principal either martensitically or by a nucleation and growth process, depending on alloy composition and cooling rate.

#### 1.4.1 Martensitic Transformations

This process involves a cooperative movement of atoms, resulting in a microscopically homogeneous tranformation of the bcc into the hcp crystal lattice. Quenching of the bcc β phase of pure Ti and dilute Ti-alloys can result essentially in two different crystal structures of athermal martensites: the hexagonal martensite which is designated α', and the orthorhombic martensite which is designated α". The most prevalent type is α', which can occur in two limiting morphologies: massive or lath martensite (high purity Ti and very dilute alloys) and "acicular" martensite in alloys with slightly higher solute contents. The "acicular" martensite α' occurs as an intimate mixture of indiviudal α plates, each having a different variant of the Burgers relation (Figure 7). The orthorhombic martensite α" seems to occur mainly in Ti-alloys with β stabilizers of the transition metals Mo, Nb, Ta, W, Re and in Ti-alloys with Al + V. The compositional

boundaries α'/α" differ from alloy system to alloy system [e.g. 11]. The lattice parameters of α" are strongly dependent on solute content, and the α" crystal structure is sometimes conveniently viewed as a distorted hexagonal structure.

### 1.4.2 Nucleation and Diffusional Growth

In Ti-alloys with intermediate solute contents, which are cooled with sufficiently low rates from the single β phase field into the α+β field, the β phase decomposes by nucelation of α at β grain boundaries and subsequent diffusion controlled growth into the retained β phase. The resulting microstructure consists of colonies of parallel α plates which are separated by plates of the retained β phase., The α plates within a colony all have the same crystallographic orientation which belongs to a single variant of the Burgers orientation relation with regard to the parent β matrix. An example of such a microstructure which was obtained by slow cooling from the β phase field is shown in Figure 8. For Ti-alloys with higher β stabilizing alloy contents and therefore decreasing transformation temperatures the colonies become progressively smaller, exhibit fewer platelets, and appear to nucleate indepentently of the β grain boundaries. The distribution of these smaller colonies over all possible variants of the Burgers orientation relationship results in a characteristic microstructure which is called "basket-weave" structure.

## 1.5 Alloy Classification

Commercial titanium alloys are classified conventionally in three different categories as α, α+β, and β alloys according to their equilibrium constitution, which varies with the types and concentrations of alloy elements. This is shown in a schematical pseudobinary β-isomorphous phase diagram in Figure 9. A listing of various commercial alloys, belonging to one of the three groups, is shown in Table 3. Commercial purity titanium having various amounts of interstitial oxygen to increase the yield stress and alloys with α stabilizers (Al, Sn) are of the hcp crystal structure at low temperature and as such classified as α alloys. The majority of the commercial alloys in Table 3 belongs to the α+β alloys. These alloys contain, in addition to the α stabilizer Al, also β stabilizing elements such as V, Mo, Nb or Cr. These elements decrease the α/β transformation temperature and increase the width of the α+β phase field with increasing β-solute content. Furthermore they lower the temperature, where the β phase starts to transform by the martensitic process ($M_s$-temperature). With a further increase in β stabilizing elements, beyond that content which lowers the $M_s$-temperture to RT, those alloys are then called metastable β alloys. For these alloys the β phase can be retained at RT even in large sections during air cooling. However, these metastable β alloys can usually be tranformed to a α+β mixture by isothermal aging. At even higher β stabilizer contents the alloys are stable β alloys, which cannot be transformed to an α+β mixture by further heat treatments.

| Code/Designation | Alloy Composition (wt.%) | $T_\beta$ (°C) |
|---|---|---|
| α-alloys | | |
| Grade 1 | CP-Ti (0.2 Fe, 0.18 O) | 890 |
| Grade 2 | CP-Ti (0.3 Fe, 0.25 O) | 915 |
| Grade 3 | CP-Ti (0.3 Fe, 0.35 O) | 920 |
| Grade 4 | CP-Ti (0.5 Fe, 0.40 O) | 950 |
| Grade 6 | Ti-5Al-2.5Sn | 1040 |
| Grade 7 | Ti-0.2Pd | 915 |
| Grade 12 | Ti-0.3Mo-0.8Ni | 880 |
| α + β alloys | | |
| Ti-8-1-1 | Ti-8Al-1V-1Mo | 1040 |
| Ti-11 | Ti-6Al-2Sn-1.5Zr-1Mo-0.35Bi-0.1Si | 1015 |
| TIMETAL 1100 | Ti-5.9Al-2.6Sn-3.8Zr-0.4Mo-0.45Si | 1010 |
| IMI 679 | Ti-2.5Al-11Sn-5Zr-1Mo-0.2Si | 945 |
| IMI 685 | Ti-6Al-5Zr-0.5Mo-0.25Si | 1020 |
| IMI 829 | Ti-5.5Al-3.5Sn-3Zr-1Nb-0.25Mo-0.3Si | 1015 |
| IMI 834 | Ti-5.8Al-4Sn-3.5Zr-0.5Mo-0.7Nb-0.35Si-0.06C | 1045 |
| Ti-56-21-S | Ti-5Al-6Sn-2Zr-0.8Mo-0.25Si | 1005 |
| Ti-6-2-4-2 | Ti-6Al-2Sn-4Zr-2Mo-0.1Si | 995 |
| Ti-55-22-S | Ti-5Al-5Sn-2Zr-2Mo-0.25Si | 980 |
| Ti-3-2.5 | Ti-3Al-2.5V | 935 |
| Ti-6-4 | Ti-6Al-4V | 995 |
| Ti-6-6-2 | Ti-6Al-6V-2Sn | 945 |
| IMI 550 | Ti-4Al-2Sn-4Mo-0.5Si | 975 |
| Ti-55-24-S | Ti-5Al-5Sn-2Zr-4Mo-0.25Si | 960 |
| Ti-6-Q2 | Ti-6Al-2Sn-2Zr-2Mo-2Cr-0.25Si | 970 |
| Ti-6-2-4-6 | Ti-6Al-2Sn-4Zr-6Mo | 940 |
| TIMETAL 62S | Ti-6Al-2Fe-0.1Si | 1015 |
| Corona 5 | Ti-4.5Al-5Mo-1.5Cr | 935 |
| Ti-17 | Ti-5Al-2Sn-2Zr-4Mo-4Cr | 890 |
| Metastable β-Alloys | | |
| B 120 VCA | Ti-13V-11Cr-3Al | 720 |
| Beta III | Ti-11.5Mo-6Zr-4.5Sn | 760 |
| Beta C | Ti-3AL-8V-6Cr-4Mo-4Zr | 795 |
| TIMETAL 10-2-3 | Ti-10V-2Fe-3Al | 800 |
| TIMETAL 15-3 | Ti-15V-3Cr-3Al-3Sn | 760 |
| TIMETAL 21S | Ti-15Mo-2.7Nb-3Al-0.2Si | 815 |
| TIMETAL LCB | Ti-4.5Fe-6.8Mo-1.5Al | 810 |
| Beta-CEZ | Ti-5Al-2Sn-2Cr-4Mo-4Zr-1Fe | 890 |
| SP 700 | Ti-4.5Al-3V-2Mo-2Fe | 900 |

Table 3: Titanium Alloys

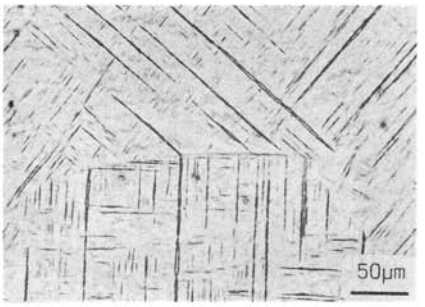


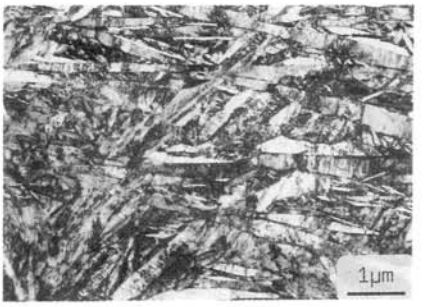


a) LM b) TEM

Fig. 7: "Acicular" martensite in Ti-6Al-4V quenched from the β phase field.

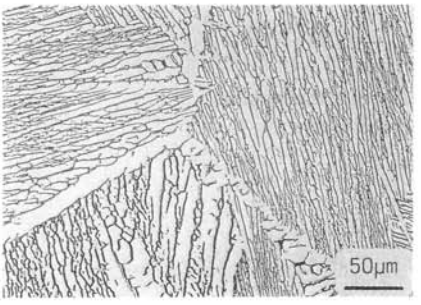


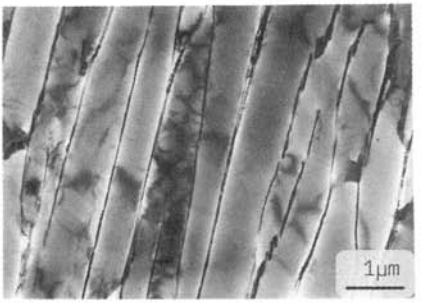


a) LM b) TEM

Fig. 8: Lamellar α+β microstructure in Ti-6Al-4V slowly cooled from the β phase field.

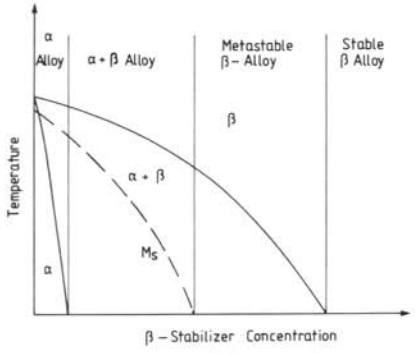


Fig. 9: Pseudobinary β isomorphous equilibrium phase diagram (schematically).

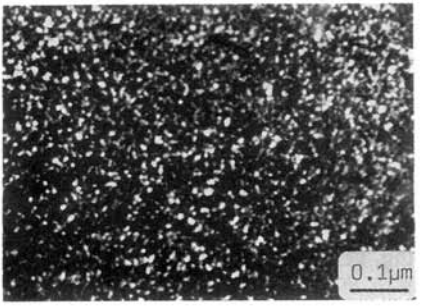


Fig. 10: Darkfield micrograph of $\alpha_2$ precipitates in the Ti-alloy IMI 834 aged 2h at 700°C (TEM).

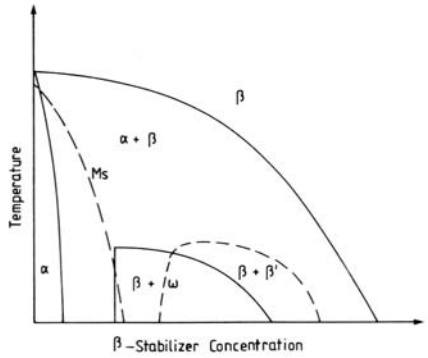


Fig. 11: Metastable β + ω and β + β' phase fields within β-isomorphous equilibrium phase diagram (schematically).

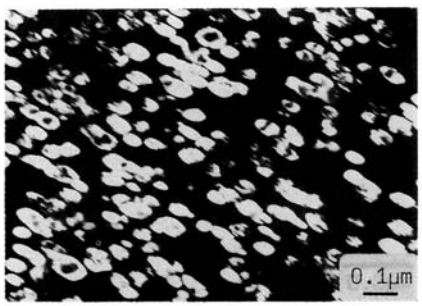


Fig. 12: Dark field micrograph of ω precipitates in the Ti-16Mo alloy aged for 48h at 450°C (TEM).

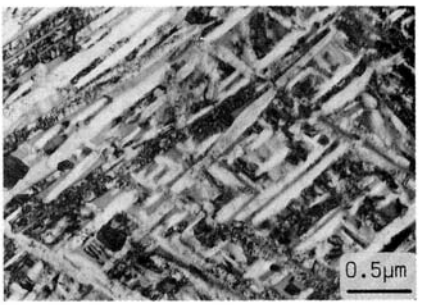


Fig. 13: Bright field micrograph of α platelets in the Ti-alloy β-CEZ aged for 8h at 580°C (TEM).

### 1.6 Basic Hardening Mechanisms

The very high yield stresses which can be obtained in commercial Ti-alloys are mainly resulting from the precipitation of finely dispersed particles in the α and β phases by suitable age-hardening treatments after cooling the alloys from their respective annealing temperatures to RT. All these alloys are of course additionally solid solution strengthened by interstitial or substitutional atoms.

#### 1.6.1 Hardening of the α phase

Pure α Ti-alloys are used in commercial application in the solid solution strengthened condition. CP-Ti has various amounts of interstitional oxygen levels, ranging from 1800 to 4000 ppm (Table 3), which results in pronounced increases in yield stress values, while other α-alloys are strengthened by substitutional atoms such as Al in combination with Sn (e.g. Ti-5Al-2.5Sn). The deformation behavior of the solid solution strengthened α phase changes with increasing solute content from a wavy to a more planar dislocation distribution, probably due to short-range ordering of the solute atoms.

Commercial α+β alloys normally have higher Al-contents (about 5 to 6 wt.%), together with increasing concentrations of β stabilizers (Table 3). Due to alloy element partitioning during annealing treatments, the α phase in these alloys is now enriched in α stabilizing elements (e.g. Al), which allows the precipitation of $\alpha_2$ particles by suitable heat treatments in the $\alpha+\alpha_2$ phase field. The $\alpha_2$ phase is ordered, based on the composition $Ti_3Al$ and has a $DO_{19}$ structure. The $\alpha_2$ particles are coherent with the α matrix and are sheared by moving dislocations, resulting in a planar dislocation distribution. When large, these $\alpha_2$ particles have an ellipsoidal morphology, the long axis being parallel to $[0001]_\alpha$. The very high density of these homogeneously distributed $\alpha_2$ particles in the α phase of the Near-α alloy IMI 834 are shown in the dark field micrograph in Figure 10.

#### 1.6.2 Hardening of the β phase

The decomposition of the β phase in α+β or metastable β alloys will be shown by the schematic phase diagram in Figure 11 [21]. There are two metastable phases, ω and β', which are observed in the β phase of sufficiently fast cooled and subsequently aged α+β or metastable β alloys. The ω phase occurs in alloys with intermediate β stabilizer contents during aging at temperatures up to 550 °C. This isothermal $\beta \rightarrow \omega$ transformation occurs most rapidly of all β phase decomposition processes by a displacement controlled transformation [22]. The morphology of ω appears as ellipsoidal particles in alloys with Mo or Nb, and as cuboidal particles in those with V or Cr. An example of ω particles in Ti-Mo is shown in the dark field micrograph in Figure 12. The ω phase is coherent or semicoherent with the β matrix and results therefore in a planar dislocation distribution, which favors early crack nucleation by grain boundary shearing and concomittant loss in ductility [23]. Since the ω phase is lean in β solutes, it can act as

nucleation sites for the formation of the equilibrium α phase, at longer aging times.

The β' phase occurs in the temperature range from 200 to 500 °C as coherent bcc zones in the matrix. It is viewed as a phase separation reaction occurring in a wide range of alloy systems which contain suffficient β stabilizer to preclude ω phase formation and where the direct $\beta \rightarrow \alpha$ transformation is too slow. There is almost no increase in yield stress observed as a result of β' precipitation. However, the β' phase can also serve as nucleation sites for the equilibrium α phase formation, since β' is also lean in β solutes.

The equilibrium α phase can also be formed directly from the β phase in concentrated alloys aged above the maximum temperature for ω formation. In such cases the α phase forms as plates or needles, each being a single variant of the Burgers orientation relation. An example of this type of α phase is shown in Figure 13. This direct formation of α in β frequently results in an inhomogeneous distribution and in relatively coarse α plate sizes, resulting only in a limited increase in yield stress. A more homogeneous distribution of α particles and therefore a much higher yield strength can be obtained by cold working prior to aging, which results in heterogeneous nucleation of α at dislocations. Another possibility to obtain a more homogeneous α particle distribution consists of two-step aging procedures to precipitate first ω or β' at lower temperatures, which than serve as nucleation sites for α formation during the second aging step at slightly higher temperatures. This also improves the yield stress.

### 1.7 Basic Physical and Chemical Properties

Some selected physical properties are summarized for comparison reasons for polycrystalline high-purity α-Ti and a commercial β Ti-alloy in Table 4.

| Property | α-Ti (> 99.9 wt. %) | β Ti-15-3 |
|---|---|---|
| Linear Expansion Coefficient | $8.36 \cdot 10^{-6}$ $K^{-1}$ | $8.5 \cdot 10^{-6}$ $K^{-1}$ |
| Thermal Conductivity | 14.99 W/m · K | 8.08 W/m · K |
| Specific Heat Capacity | 523 J/kg · K | 500 J/kg · K |
| Electrical Resistivity | $5.6 \cdot 10^{-7}$ Ω · m | $1.4 \cdot 10^{-6}$ Ω · m |
| β/α Transform. Temperature | 882.5 °C | 760 °C |
| Young's Modulus | 115 GPa | 82 GPa (sol. treated) |
| Shear Modulus | 44 GPa | - - |
| Poissons Ratio | 0.33 | - - |
| Density | 4.51 $g/cm^3$ | 4.7 $g/cm^3$ |

Table 4: Physical Properties of α-Ti and the β alloy Ti-15-3 at RT

The density of Ti-alloys with about 4.6 $g/cm^3$ lies between that of Al-alloys (~ 2.7 $g/m^3$) and Steels (~ 7.8 $g/m^3$). Because of the very high yield stress values which can be obtained for Ti-alloys (similar to steels and about twice that of high-strength Al-alloys) the resulting high yield stress to weight ratios are favoring the application of Ti-alloys in many areas where weight savings are of predominant importance.

### 1.7.1 Diffusion

Although there exist many published data on the diffusivities of various interstitial and substitutional elements in Ti, the results in many cases are exhibiting pronounced scattering. Nevertheless, a few general remarks will be summarized on the basis of the Arrhenius plots shown in Figure 14. This diagram serves only as a rough estimation and will be considered more as a schematic drawing. For detailed diffusivities the original literature has to be contacted [e.g. 24]. The self diffusion coefficients of bcc β-Ti are at least two orders of magnitude higher as compared to those in hcp α-Ti, which is the main reason for applying Near-α Ti-alloys as creep resistant high-temperature alloys instead of β Ti-alloys. The interstitial elements, such as O and N, are diffusing much faster than substitutional elements, such as Al, V or Mo. Very high diffusion rates are reported for interstitial hydrogen, which has serious consequences for applications of Ti-alloys in aqueous or humid gaseous environments, especially under high static loads (stress corrosion cracking) or fatigue loading (corrosion fatigue), because of hydrogen embrittlement.

### 1.7.2 Oxidation

The oxidation product during air exposure observed on Ti and its conventional alloys is essentially $TiO_2$ with a tetragonal rutile crystal structure, which is called scale. This layer is an n-type anion-defective oxide through which the oxygen ions can diffuse. The scale therefore grows into the base metal, which for example prevents the self-healing of cracks in Ti. The driving force for the rapid oxidation of Ti is the high chemical affinity between Ti and oxygen (higher than between Ti and N). This, together with the high maximum solubility of oxygen in Ti of about 14.3 wt.% results during oxydation in the simultaneous formation of the scale and an adjacent inner layer of the base metal, which is highly enriched in oxygen, called α-case. As mentioned in Section 1.6, the deformation behavior of α-Ti changes from a wavy to a planar mode with increasing oxygen levels. Therefore, the hard, less ductile α-case induces surface cracks under tension loading which results in low overall ductilities or causes early crack nucleation under fatigue loading because of large slip offsets at the surface. The application of conventional Ti-alloys at higher temperatures is therefore limited to the regime below about 550 °C where the diffusion rates through the oxide layer (scale) are low enough to prevent excess oxygen contents being dissolved in the bulk material. At temperatures above about 550°C the $TiO_2$ scale can be dissolved if further oxidation is simultaneously prevented by heating the material either in vacuum or in a protective atmosphere. This forms the basis of joining Ti-alloys by the diffusion bonding process (see Section 4.3).

In order to decrease the diffusion rate of oxygen through the scale, various additions of alloy elements were investigated. Slight improvements were found by adding elements with a valency greater than 4, such as $Nb^{5+}$, which can substitute the $Ti^{4+}$ ions in the $TiO_2$ structure, thus reducing the number of anion vacancies. However, much more effective in

lowering the diffusion rates are inceasing amounts of Al, which forms the very dense and thermally stable $\alpha$-$Al_2O_3$ oxide. The resulting scale consists then of a heterogeneous mixture of $TiO_2$ and $Al_2O_3$ underneath a $TiO_2$ surface oxide, as shown in the schematic diagram in Figure 15 [25]. The improved oxidation resistance of titanium aluminides, such as $Ti_3Al$ based alloys or $\gamma$-TiAl, results from increasing volume fractions of $Al_2O_3$ oxide in the scale. Due to the higher Al content $\gamma$-TiAl exhibits a better oxidation resistance as compared to alloys based on $Ti_3Al$. However, for surface protection by a continuous $Al_2O_3$ layer even higher concentrations of about 57 at.% Al would be required (Figure 15).

### 1.7.3 Corrosion Behavior

The excellent resistance of Ti and its alloys to most environments is the result of the protective surface film, which consists basically of $TiO_2$. Although titanium is chemically very reactive, this thin oxide film passivates the base metal, as long as its integrity can be maintained. In general this is the case in most oxidizing environments, for example in salt solutions, including chlorides, hypochlorides, sulfates and sulfides or in nitric acid solutions. On the other hand, titanium is not corrosion resistant under reducing conditions, in very powerful oxidizing environments or in the presence of fluoride ions, where the protective nature of the oxide film diminishes. The stability and integrity of the film can be improved, however, if inhibiting additions can be added to these environments.

Ti-alloys which are subjected simultaneously to mechanical stresses and aggressive environments can be severely influenced by hydrogen embrittlement or stress corrosion cracking. It is known that $\alpha$ and $\alpha+\beta$ alloys are more prone to such brittle fracture, while $\beta$ alloys are more tolerable, that means the bcc phase can tolerate higher concentrations of hydrogen before brittle fracture occurs, while in the hcp phase already low concentrations of hydrogen can result in brittle fracture mainly along the basal planes.

## 2. Thermomechanical Processing and Microstructure

The microstructure of Ti alloys can be varied and controlled by thermomechanical processing. The nature and degree of microstructure control that can be obtained depends on the alloy class and type. This section will describe the effects of thermomechanical processing on microstructure of Ti alloys.

### 2.1 CP Titanium

The thermomechanical processing of commercially pure (CP) titanium is usually perfomed completely in the $\alpha$ phase field (Figure 16) and the main goal from the microstructural viewpoint is the adjustment of the $\alpha$ grain size to the desired level. Due to the good formability of CP titanium the deformation step is performed at relatively

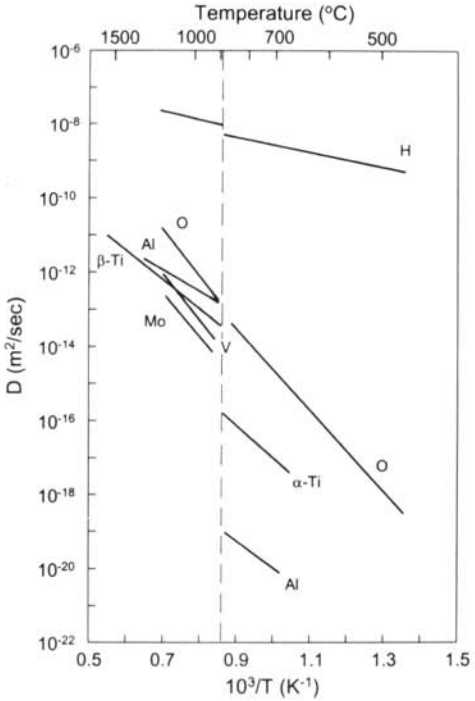


Fig. 14: Temperature dependence of approximated diffusion coefficients for self diffusion and for various alloying elements in Titanium.

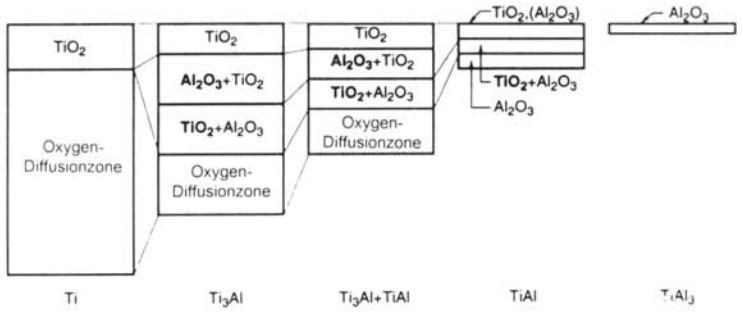


Fig. 15: Schematic cross sections through the oxide layers and oxygen diffusion zones in Titanium and Titanium Aluminides [25].

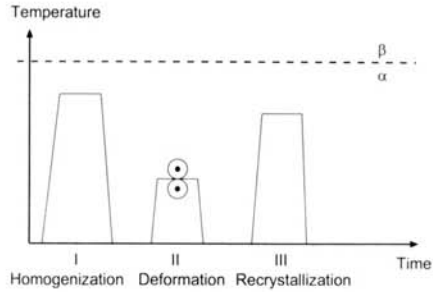


Fig. 16: Processing route for CP Titanium (schematically).

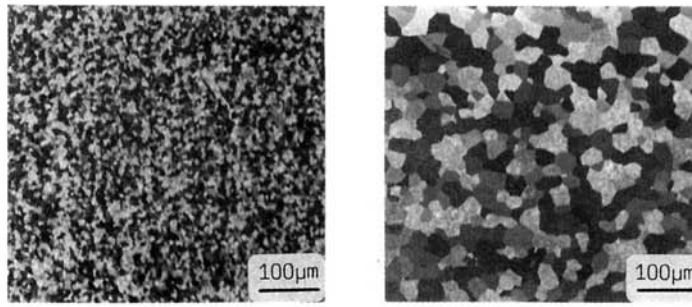


a) Grain size ~ 10µm b) Grain size ~ 50µm

Fig. 17: Grain structure of CP Titanium.

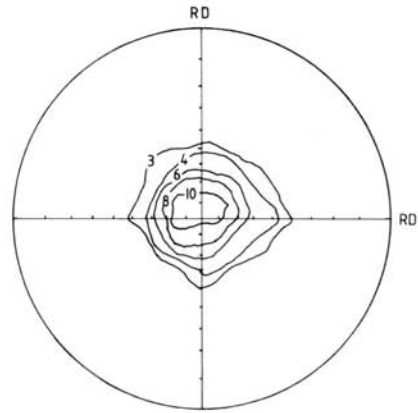


Fig. 18: (0002) pole figure of CP Titanium.

low temperatures (200-300°C) and even room temperature deformation (cold deformation) is possible. The formability is decreasing with increasing oxygen level from Grade 1 to Grade 4 because with increasing oxygen the ease of twinning is decreased. The desired α grain size can be adjusted by choosing the temperature for the recrystallization treatment. For example, small α grain sizes (10μm) can be reached by recrystallization around 700-750°C whereas larger α grain sizes (50μm) can be obtained by recrystallization around 900 °C (Figure 17).

Besides oxygen level and α grain size, the crystallographic texture of the hexagonal α phase developed during the deformation step and not changed significantly by the recrystallization is a third parameter important for the mechanical properties of CP titanium. Colled rolled CP titanium sheets, for example, exhibit a strong, so-called "basal" texture (Figure 18) in which the basal planes are aligned parallel to the sheet plane.

## 2.2 Alpha + Beta Alloys

In the two phase α+β titanium alloys three distinctly different types of microstructures can be obtained by changing the thermomechanical processing route: a fully lamellar structure, a fully equiaxed structure, and a so-called duplex or bi-modal microstructure containing equiaxed primary α in a lamellar α+β matrix.

### 2.2.1 Bi-Modal Microstructures

A typical processing route for obtaining the so-called bi-modal (duplex) microstructure is shown schematically in Figure 19, dividing the process into four different steps: homogenization in the β phase field (I), deformation in the α+β phase field (II), recrystallization in the α+β phase field (III), and aging at lower temperatures (IV). The important parameters for each of these four steps as well as the resulting microstructural features are shown in a tabulated form in Figure 20. The most critical parameter in step I is the cooling rate from the homogenization temperature determining the width of the α-lamellae in the lamellar structure within the β grains and the extent of the continuous α-layer at β grain boundaries. Figure 21 shows examples for cooling rates of 1 °C/min, 100 °C/min, and 8000 °C/min. The β grain size is always fairly large (500 μm and larger) even if the homogenization temperature is kept as low and the homogenization time as short as possible from a practical standpoint. By the next step (II), the deformation process in the α+β phase field, the lamellar structure is deformed plastically (not broken up). The plastic deformation should be as high as possible but should at least introduce enough dislocations to obtain complete recrystallization of the α and β phases during step III. During the deformation process in step II, crystallographic textures in the hexagonal α phase and in the bcc β phase can develop. Figure 22 shows schematically the different textures which can be formed. The deformation temperature determines the texture type. At "low" deformation temperatures (a high volume fraction

of α phase is present during deformation) an α-deformation texture, a so-called basal/transverse (B/T) type of texture, develops whereas at "high" deformation temperatures in the α+β phase field (a high volume fraction of β phase is present during deformation) a β-deformation texture develops in which, upon subsequent transformation to α, only one of the six possible variants of the Burgers-relationship, (110) // (0002), is selected, resulting in a so-called transverse (T) type of transformation texture. The deformation degree determines the texture intensity whereas the deformation mode (unidirectional rolling, cross-rolling, pancake forging, etc.) determines the texture symmetry (Figure 22). The resulting textures of the hexagonal α phase will not change significantly during the subsequent recrystallization step III.

Important parameters of this recrystallization step III are the temperature, which determines the volume fraction of recrystallized equiaxed $\alpha_p$ located at the "triple-points" of the recrystallized equiaxed β grains, and the cooling rate from the recrystallization temperature, which determines the width of the individual α lamellae as well as the α colony size of the lamellar structure formed during cooling within the equiaxed β grains. A typical example of the resulting bi-modal structure can be seen in Figure 23b. The mechanism by which the lamellar "starting" structure (step I, Figure 21), being deformed in step II, is changed to equiaxed α and β grains during the recrystallization process is illustrated in Figure 24a. It can be seen that the recrystallized β phase penetrates into the recrystallized α lamellae along α/α grain boundaries causing the separation into individual $\alpha_p$ grains.

It should be pointed out that if the cooling rate from the recrystallization temperature is sufficiently low, only the $\alpha_p$ grains will grow and no α lamellae are formed within the β grains, resulting in a so-called globular (fully equiaxed) structure with the equilibrium volume fraction of β grains located at the "triple-points" of the α grains (Figure 25). This globular microstructure is also formed when the recrystallization temperature is sufficiently low, for example 800 °C for Ti-6Al-4V. In this case, the mechanism that changes the deformed lamellar "starting" structure to equiaxed grains is the reverse: α phase penetrates along β/β grain boundaries into the recrystallized β-lamellae (Figure 24b).

The resulting $\alpha_p$ size is influenced mainly by the width of the α lamellae of the "starting" structure, which depends on the cooling rate from the β phase field in step I (Figures 19 and 20). This is illustrated by the comparison of Figures 23b and c, the only difference in the processing route being the cooling rate after the β homogenization heat treatment (step I) during a compressor disk fabrication process. Figure 23a shows, for comparison, the microstructure of a fully lamellar compressor disk which will be discussed later on.

It should be pointed out that the recrystallization time during step III is not very critical (Figure 20), as long as the time is sufficient for the generation of equiaxed and isolated $\alpha_p$ grains, because grain growth is very sluggish in these two-phase mixtures of α and β grains.

The combination of $\alpha_p$ volume fraction (recrystallization temperature) and $\alpha_p$ size

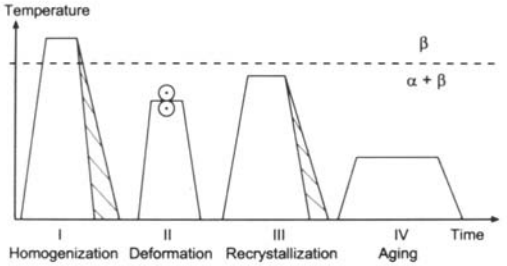


Fig. 19: Processing route for bi-modal microstructures of (α+β) Ti-alloys (schematically).

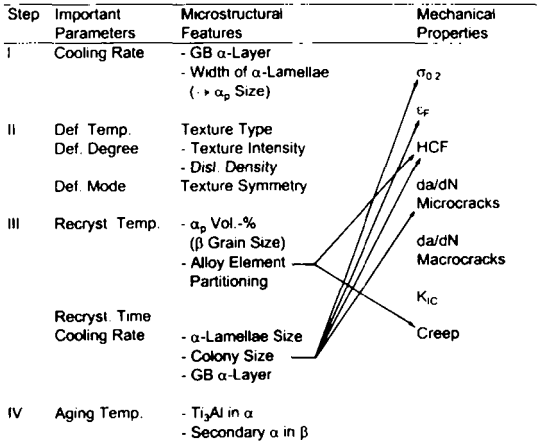


Fig. 20: Important processing parameters, resulting microstructural features, and major influences on mechanical properties (arrows) for bi-modal microstructures.

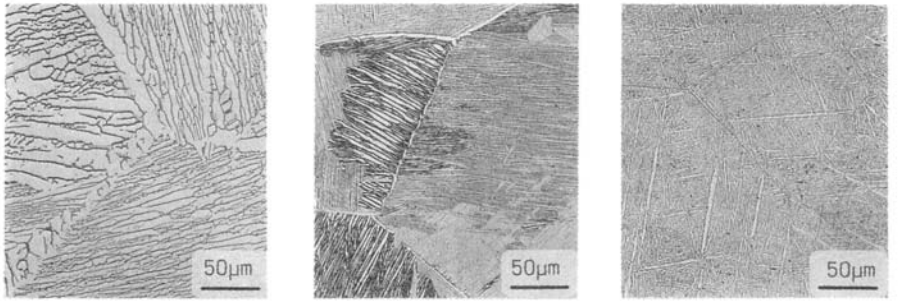


a) 1°C/min b) 100°C/min c) 8000°C/min

Fig. 21: Effect of cooling rate from the β phase field on lamellar microstructures, Ti-6242.

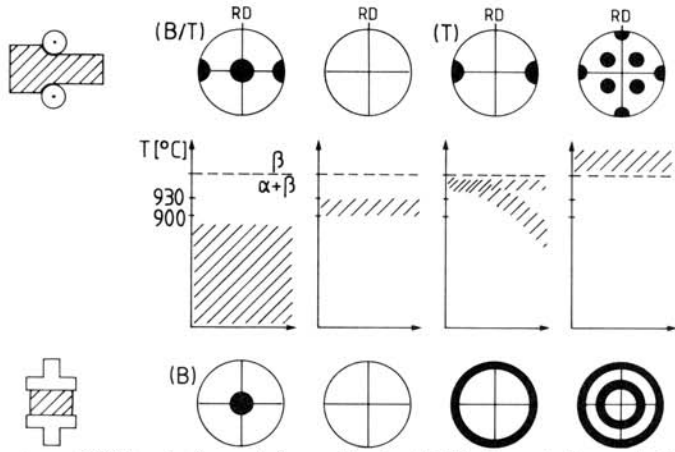


Fig. 22: Textures (0002 pole figures) formed in (α+β) Ti-alloys (schematically).

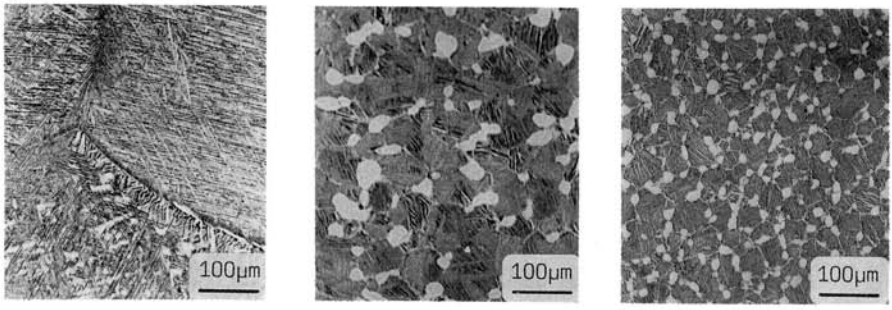


a) Lamellar b) Bi-modal 1 c) Bi-modal 2

Fig. 23: Microstructures, IMI 834.

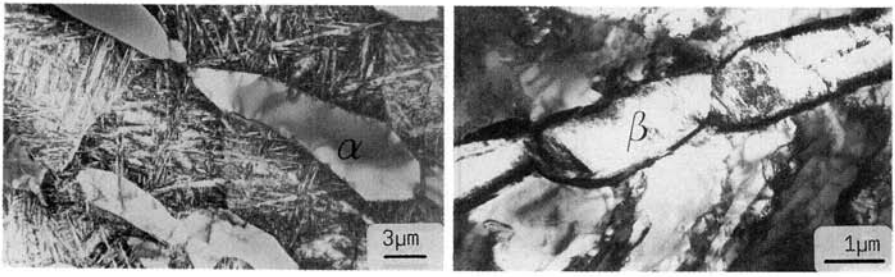


a) 950°C b) 800°C

Fig. 24: Recrystallization to a bi-modal structure (950°C) and to a fully equiaxed structure (800°C), TEM, Ti-6Al-4V.

(cooling rate after β homogenization) defines an important parameter, namely the β grain size (distance between $\alpha_p$ grains), which limits the maximum α colony size.

Upon separation into $\alpha_p$ and β those alloying elements which are either strong α-stabilizers (for example Al, oxygen) or strong β-stabilizers (for example Mo, V) will partition respectively into the two phases. This alloy element partitioning effect has the consequence that the α lamellae formed from the β phase upon cooling, have a lower concentration of elements (especially oxygen) which are promoting age-hardening by formation of coherent $Ti_3Al$ particles in step IV as compared to $\alpha_p$.

In step IV the temperature is more important than the time (Figure 20) because the temperature being either below or above the $Ti_3Al$ solvus temperature determines whether age-hardening by $Ti_3Al$ particles occurs in the α phase or not. For example, for the Ti-6Al-4V alloy the $Ti_3Al$ solvus temperature is about 550 °C. This means aging at 500 °C will precipitate $Ti_3Al$ particles whereas a heat treatment at 600 °C or above will be only a stress relieving treatment. For Ti-6242 ($Ti_3Al$ solvus about 650 °C) and IMI 834 ($Ti_3Al$ solvus about 750 °C) the recommended final heat treatment temperatures (590 °C and 700 °C, respectively) will cause age-hardening by $Ti_3Al$ particles. It should be pointed out, that with respect to the formation of $Ti_3Al$ particles the alloying elements Al and Sn are additive.

In addition, depending on the details of step III (recrystallization temperature and cooling rate), fine secondary α can be precipitated in the β phase during the heat treatment in step IV. In all cases the residual stresses which can form as a result of relatively fast cooling rates in step III are relieved by the heat treatment in step IV. If this final heat treatment in step IV is used only for stress relieving (temperature above $Ti_3Al$ solvus) it is called mill-annealed condition (see Section 4.3).

### 2.2.2 Fully Lamellar Microstructures

For some applications a so-called fully lamellar microstructure is produced. The processing route for obtaining these fully lamellar microstructures is shown in Figure 26 and the important parameters are listed in Figure 27 together with the resulting microstructural features. In this case, a homogenization treatment in the β phase field (step I in Figure 26) is applied after deformation either in the α+β phase field or in the β phase field. The cooling rate from the homogenization temperature is now extremely important because it determines the final lamellar structure (α lamellae size, α colony size) and the extent of α-layers at β grain boundaries (see Figure 21). After step I only step IV, the aging treatment or the stress relieving treatment, is normally applied. Since no alloy element partitioning effect is present for the fully lamellar structure, the degree of age-hardening by $Ti_3Al$ particles is usually higher than for the lamellar portion of the bi-modal microstructure.

It should be pointed out, that for β processed material step I can be deleted completely and step IV can be applied directly after β deformation. In that case, the extent of α-layers at β grain boundaries can be reduced and modified but this process is

more difficult to control in a reproducible way as compared to β annealed conditions.

## 2.3 Beta Alloys

Beta alloys by definition do not transform martensitically upon cooling from the β phase field to room temperature. As a result, these alloys are somewhat simpler to describe from a microstructural viewpoint than α+β alloys. Depending on the amount of β stabilizing elements, these β alloys can be retained in a metastable form upon cooling to room temperature at moderate to high cooling rates, that means no significant precipitation of α phase is taking place during the cooling process. In that state the alloys are easy to deform at relatively low temperatures and for many β alloys "cold" deformation at room temperature is possible (step II in the schematical processing route, Figure 28).

### 2.3.1 Beta Annealed Microstructures

If the recrystallization process after deformation is performed in the β phase field (step III, Figure 28) the microstrucure after step III is similar to the microstructure after step I, maybe with a somewhat reduced equiaxed β grain size. Upon aging in the α+β phase field the α phase is precipitating in the β matrix in form of α plates. For many β alloys a two-step aging treatment is performed (step IVa and IVb in Figure 28). The first step is done at relatively high temperatures forming coarse α plates (Figure 29a, LM) and the second step at low temperature forming fine α platelets in between the coarse α plates (Figure 29b, TEM).The presence of ω and β' precipitates (see Section 1.6.2) is normally completely avoided in β alloys because these shearable precipitates can cause brittle behavior on a macroscopic scale in these relatively coarse grained β alloys. But as pointed out already in Section 1.6.2 these coherent precipitates are useful as precursors, nucleated either during pre-aging at lower temperatures or during the cooling and heating process, leading to a homogeneous distribution of α platelets.

The microstructural problem associated with these β annealed conditions can be seen in Figure 29a. A continuous α layer is formed along β grain boundaries due to preferrential precipitation of the incoherent α phase at β grain boundaries. These continuous α layers have a strong negative influence on the ductility of these β annealed conditions (see Section 3.2). To avoid this negative influence, two different approaches have been taken for β alloys [26]. One approach is to obtain a bi-modal microstructure similar to the bi-modal (duplex) microstructure in α+β alloys (Section 2.3.2) and the other approach is to create a so-called necklace type of microstructure (Section 2.3.3).

### 2.3.2 Bi-Modal Microstructures

The thermomechanical processing route to obtain a bi-modal microstructure (Figure 30) is shown schematically in Figure 31. Upon heating of the deformed condition in the

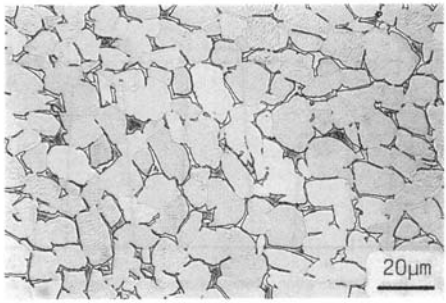


Fig. 25: Fully equiaxed microstructure, LM, Ti-6242.

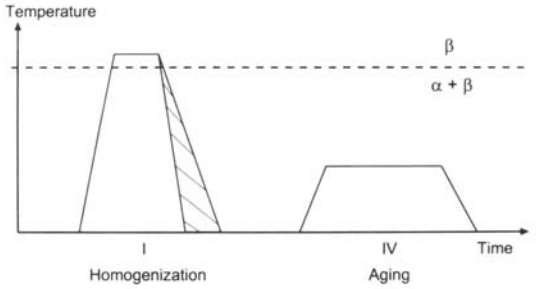


Fig. 26: Processing route for fully lamellar microstructures of (α+β) Ti-alloys (schematically).

| Step | Important Parameters | Microstructural Features | Mechanical Properties |
|---|---|---|---|
| I | Temp.<br>Cooling Rate | Large β Grain Size<br>- α-Lamellae Size<br>- Colony Size<br>- GB α-Layer | $\sigma_{0.2}$<br>$\varepsilon_f$<br>HCF |
| IV | Aging Temp. | - $Ti_3Al$ in α<br>- Secondary α in β | da/dN Microcracks<br>da/dN Macrocracks<br>$K_{IC}$<br>Creep |

Fig. 27: Important processing parameters, resulting microstructural features, and major influences on mechanical properties (arrows) for fully lamellar microstructures.

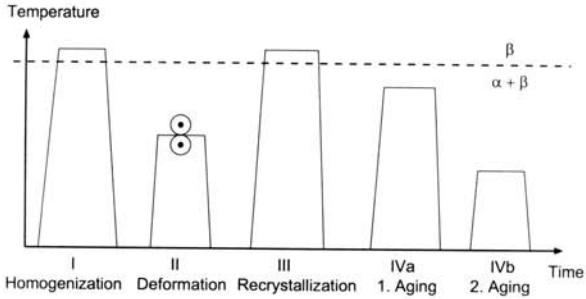


Fig. 28: Processing route for β annealed (lamellar) microstructures of β Ti-alloys (schematically).


a) LM


b) α-platelets, TEM

Fig. 29: Lamellar microstructure, β-CEZ.


Fig. 30: Bi-modal microstructure, LM.

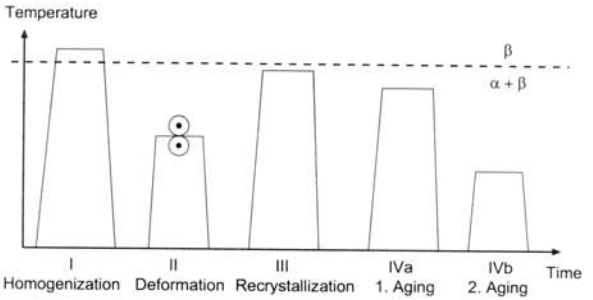


Fig. 31: Processing route for bi-model microstructures of β Ti-alloys (schematically).

$\alpha+\beta$ phase field, the $\alpha$ phase will form as round equiaxed particles and not as plates. Adjusting the annealing temperature to a relatively low volume fraction of equiaxed $\alpha$ particles (primary $\alpha$, $\alpha_p$), limiting grain growth of the $\beta$ phase during recrystallization, will create a microstructure during step III in Figure 31 which consists of equiaxed $\alpha_p$ particles and equiaxed $\beta$ grains with a grain size about equal to the interparticle $\alpha_p$ spacing (Figure 30). Steps II and III have to be repeated at least twice to create an acceptable microstructure. The double aging treatment will result in the same precipitation processes (continuous $\alpha$ layer at $\beta$ grain boundary, coarse $\alpha$ plates and fine $\alpha$ platelets within the $\beta$ grains) as described before for the $\beta$ annealed condition but the length of the continuous $\alpha$ layers is much shorter as well as the length of the coarse $\alpha$ plates due to the smaller $\beta$ grain size (Figure 30) as compared to the $\beta$ annealed condition (Figure 29a).

### 2.3.3 Necklace Microstructures

To create a necklace type of microsturcture (Figure 32) a so-called "through-transus" deformation process has to be applied (Figure 33, schematically). After homogenization the material is not cooled to room temperature but directly deformed starting in the $\beta$ phase field and continued into the $\alpha+\beta$ phase field until $\alpha$ forms at the deformed $\beta$ grain boundaries (pancake or elongated $\beta$ grain shape) as round particles (Figure 32). It is important that the deformation process is finished before $\alpha$ starts to precipitate within the deformed $\beta$ grains because in that case $\alpha$ would precipitate as round particles. Upon cooling the $\beta$ grains recover and the subsequent double aging treatment will form the coarse $\alpha$ plates and fine $\alpha$ platelets as discussed before. Figure 34 shows the resulting microstructure with the equiaxed $\alpha$ particles at $\beta$ grain boundaries and the coarse $\alpha$ plates within the $\beta$ grains. It should be pointed out that the processing parameters for this "through-transus" process, especially time and finishing temperature, are difficult to control. Another variation is to deform the material completely in the $\beta$ phase field, that means the $\alpha$-GB line in Figure 33 will be crossed upon cooling or grain boundary $\alpha$ will precipitate upon the first aging step IVa, but controlling the processing parameters is also very difficult because recrystallization of the $\beta$ phase has to be avoided during cooling. The resulting microstructure for such "$\beta$ deformed" condition is characterized by short segments of "continuous" $\alpha$ layers at the serrated, deformed $\beta$ grain boundaries. Often the beginning of recrystallization is shown up as small, more equiaxed $\beta$ grains adjacent to elongated $\beta$ grain boundaries (Figure 35). Due to the pancake or elongated $\beta$ grain shape, the mechanical properties of these necklace types of microstructures will be anisotropic (see Section 3.2).

## 3. Basic Correlation between Microstructure and Mechanical Properties

The range of microstructures that can be produced in Ti alloys allows considerable lattitude in tailoring the properties. As in Section 2, the approach depends on the alloy

class and type. This section is organized accordingly to provide clarity.

### 3.1 Alpha + Beta Alloys

It is better to first discuss the fully lamellar microstructure because this allows an easier introduction to the description of the mechanical properties of the bi-modal microstructure of $\alpha+\beta$ alloys. Furthermore, from all possible correlations only those which have a major influence on the mechanical properties are discussed in detail (arrows in Figures 20 and 27). Other microstructural effects, such as for example age-hardening and oxygen, can be found in [27, 28].

#### 3.1.1 Fully Lamellar Microstructures

The most influential microstructural parameter on the mechanical properties of fully lamellar structures is the $\alpha$ colony size, determined by the cooling rate after the $\beta$ heat treatment and limited by the size of the beta grains, because it determines the effective slip length. The general effect of slip length on mechanical properties is shown schematically in Figure 36. With increasing cooling rate the colony size is decreased (decreasing slip length) and the yield stress $\sigma_{0.2}$ is increasing (Figure 37). A drastic increase in yield stress is observed when the colony structure is changed to a martensitic type of microstructure (slip length and "colony" size equal to the width of individual $\alpha$ plates). The ductility, showing with increasing cooling rate first also a normal increasing behavior (decrease in slip length, see Figure 36), passes through a maximum and is then declining drastically at high cooling rates (Figure 37). In the maximum, the fracture mechanism is changing from a ductile transcrystalline dimple type of fracture mode to a ductile intercrystalline dimple type of fracture mode along the continuous $\alpha$-layers at $\beta$ grain boundaries (Figure 38). The magnitude of the effect of these continuous $\alpha$-layers, namely the preferential plastic deformation in these areas, depends primarily on the strength difference between these areas and the matrix and on the grain boundary length ($\beta$ grain size). As will be shown later (Section 3.2), the effect of continuous $\alpha$-layers on ductility is much more pronounced for high strength $\beta$ alloys because of the higher strength difference between matrix and $\alpha$-layers for those alloys as compared to $(\alpha+\beta)$ alloys.

The HCF strength (resistance to crack nucleation), which depends primarily on the first dislocation motion and therefore in most cases on the yield stress (Figure 36), shows as a function of cooling rate a drastic increase in the fast cooling regime (Figure 39) like the yield stress in Figure 37. For the LCF strength, both the resistance to crack nucleation and the resistance to propagation of the small surface cracks (microcracks), are important. The propagation behavior of microcracks depends also on the slip length. With increasing slip length the microcrack propagation rate in these slip bands is increased exhibiting therefore a similar dependence on slip length as the ductility $\varepsilon_F$ in Figure 36 if $\Delta K_{th}$ is plotted describing the microcrack propagation behavior. In other words, colony

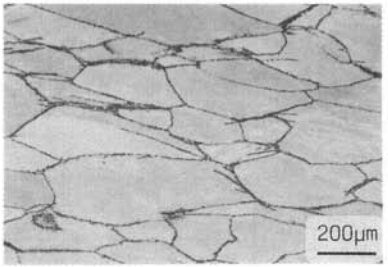


Fig. 32: Necklace microstructure after through-transus processing.

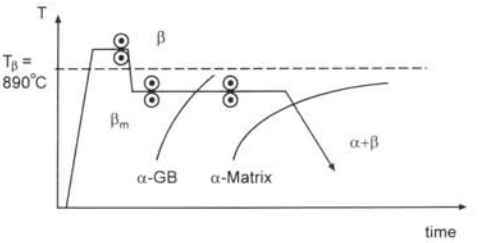


Fig. 33: Through-transus processing for necklace microstructures (schematically).

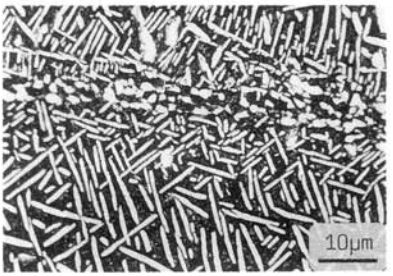


Fig. 34: Necklace microstructure, "through-transus" processing.


Fig. 35: Necklace microstructure, "β-deformed" condition, LM.

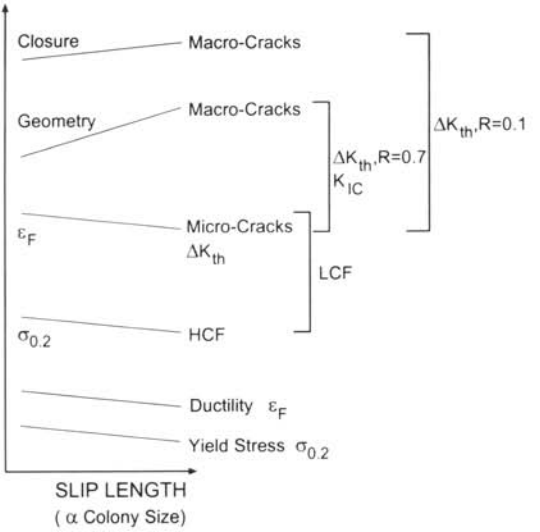


Fig. 36: Influence of slip length (α colony size) on mechanical properties (schematically)

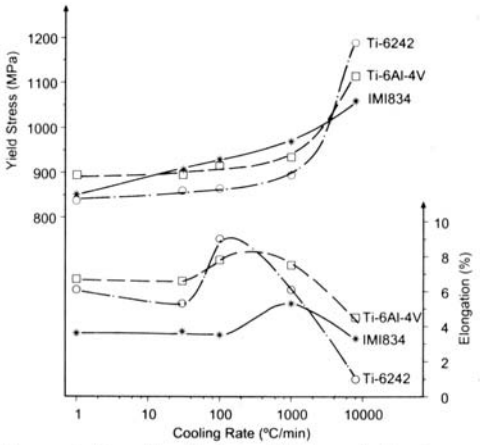


Fig. 37: Effect of cooling rate from the β phase field on yield stress and ductility of fully lamellar structures.

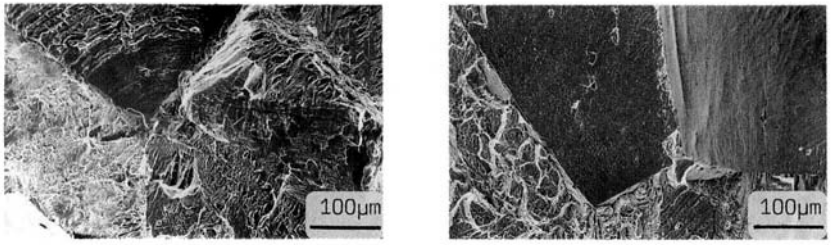


a) 100°C/min b) 8000°C/min

Fig. 38: Tensile fracture surfaces of fully lamellar structures, Ti-6242, see Fig. 37.

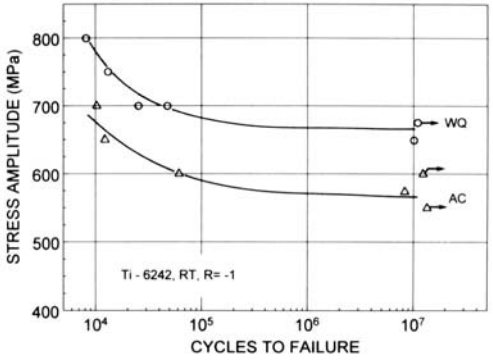


Fig. 39: S-N curves for different cooling rates of fully lamellar structures, Ti-6242.

boundaries as well as martensitic plates are strong obstacles for microcrack propagation. Figure 40 shows that with increasing cooling rate the microcrack propagation rate is decreased. The LCF strength will therefore always improve with increasing cooling rate (decreasing colony size) as shown schematically in Figure 36.

For the propagation behavior of large cracks (macrocracks), usually measured on CT-type specimens with through-thickness cracks, additional factors besides the basic microcrack propagation behavior have to be considered. At high R-ratios (no crack closure) the crack front geometry (profile) is an important additional factor. This factor also depends on slip length ($\alpha$ colony size) but with an opposite sign, that means with increasing $\alpha$ colony size this geometrical term, the crack front roughness, increases hindering crack propagation and increasing $\Delta K_{th}$ (Figure 36). Therefore, the crack propagation rate of macrocracks at high R-ratios can increase or decrease with increasing slip length ($\alpha$ colony size) depending on the slope of the two curves describing the two contributing factors with opposite sign in Figure 36. For ($\alpha$+$\beta$) titanium alloys it is usually observed that with increasing $\alpha$ colony size the propagation rate of macrocracks at high R-ratios is decreased, that means the geometrical term is stronger than the ductily term.

For the propagation behavior of macrocracks at low R-ratios crack closure can be a third contributing factor. Crack closure resulting in higher $\Delta K_{th}$ values increases with increasing roughness of the fracture surface and with increasing shear displacement at the crack tip, both increasing with slip length ($\alpha$ colony size). The resulting da/dN-$\Delta$K curves for macrocracks at low R-ratios with the three described contributions (Figure 36) show therefore even more than the curves at high R-ratios the tendency that with increasing $\alpha$ colony size (decreasing cooling rate) the propagation rate is lowered (Figure 40). The comparison of the four curves in Figure 40 is illustrating the different dependence of microcrack and macrocrack propagation behavior on cooling rate.

The dependence of fracture toughness on $\alpha$ colony size can be discussed qualitatively in a similar way as the dependence of $\Delta K_{th}$ for macrocracks without closure (Figure 36), as long as the same basic fracture mechanism is occuring in both cases. Similarly as described for the macrocracks, the fracture toughness of ($\alpha$+$\beta$) titanium alloys usually increases with increasing $\alpha$ colony size because the rougher crack front profile dominates over the ductily term. Figure 41 shows an example of this difference in crack path for a fine lamellar structure (cooling rate 8000 °C/min) and a coarse lamellar structure (cooling rate 1 °C/min). The resulting fracture toughness values are 50 and 75 MPa $\cdot$ $m^{1/2}$, respectively.

### 3.1.2 Bi-Modal Microstructures

The most influential microstructural parameter on the mechanical properties of bi-modal microstructures is the small $\beta$ grain size leading to a small $\alpha$ colony size and therefore to a short slip length. Based on the discussion of the effect of slip length on mechanical properties in the previous Section 3.1.1, it can be postulated that if the slip

length would be the only major parameter, the bi-modal microstructure should exhibit a higher yield stress, a higher ductility, a higher HCF strength, a slower crack propagation rate of microcracks and a higher LCF strength as compared to a fully lamellar microstructure, keeping the important cooling rates for the bi-modal structure (step III) and for the fully lamellar structure (step I) constant. Only the resistance to macrocrack propagation and the fracture toughness should be better for the fully lamellar structure assuming that the geometrical term in Figure 36 will overcompensate the ductily term (basic microcrack propagation resistance).

The second important parameter for the mechanical properties of bi-modal microstructures is the alloy element partitioning effect increasing with $\alpha_p$ volume fraction. This leads to a lower basic strength within the lamellar part of the bi-modal microstructure as compared to a fully lamellar structure. This alloy element partitioning effect will have a negligible influence on ductility and on the propagation behavior of microcracks and macrocracks including fracture toughness, which are then mainly determined by the first parameter, the $\alpha$ colony size.

| Microstructure | Test Temp. | $\sigma_{0.2}$ (MPa) | UTS (MPa) | $\sigma_F$ (MPa) | El. (%) | RA (%) |
|---|---|---|---|---|---|---|
| Lamellar | RT | 925 | 1015 | 1145 | 5.2 | 12 |
| Bi-modal (20% $\alpha_p$) | RT | 995 | 1100 | 1350 | 12.9 | 20 |
| Bi-modal (30% $\alpha_p$) | RT | 955 | 1060 | 1365 | 12.6 | 26 |
| Lamellar | 600°C | 515 | 640 | 800 | 10.5 | 26 |
| Bi-modal (10% $\alpha_p$) | 600°C | 570 | 695 | 885 | 9.9 | 30 |
| Bi-modal (40% $\alpha_p$) | 600°C | 565 | 670 | 910 | 14.4 | 36 |

Table 5: Tensile properties at RT and 600°C, IMI 834

The dependence of yield stress on $\alpha_p$ volume fraction is a mixture of $\alpha$ colony size effect and alloy element partitioning effect and usually shows a maximum between 10 and 20 vol.-% $\alpha_p$ (Table 5). This indicates that for small volume fractions of $\alpha_p$ the $\alpha$ colony size effect dominates, while for large volume fractions of $\alpha_p$ the alloy element partitioning effect dominates. The smaller decline in yield stress at the high test temperature of 600 °C in the high $\alpha_p$ volume fraction region (Table 5) indicates that the alloy element partitioning effect is less pronounced at high temperature, probably because the strengthening effect of oxygen is reduced. The HCF strength (crack nucleation resistance) is usually lowered with increasing $\alpha_p$ volume fraction (Figure 42). The fatigue cracks are nucleated in the lamellar grains of the bi-modal structure ( Figure 43) as a consequence of the alloy element partitioning effect resulting in a much lower basic strength of the lamellar regions as compared to $\alpha_p$. This can be fairly easily shown experimentally by microhardness measurements. The immediate decline in HCF strength with increasing $\alpha_p$ volume fraction shows that, at low stress amplitudes, the decline in basic strength of the lamellar grains (alloy element partitioning effect) is a stronger effect than the positive contribution due to the reduced $\alpha$ colony size. At the high test

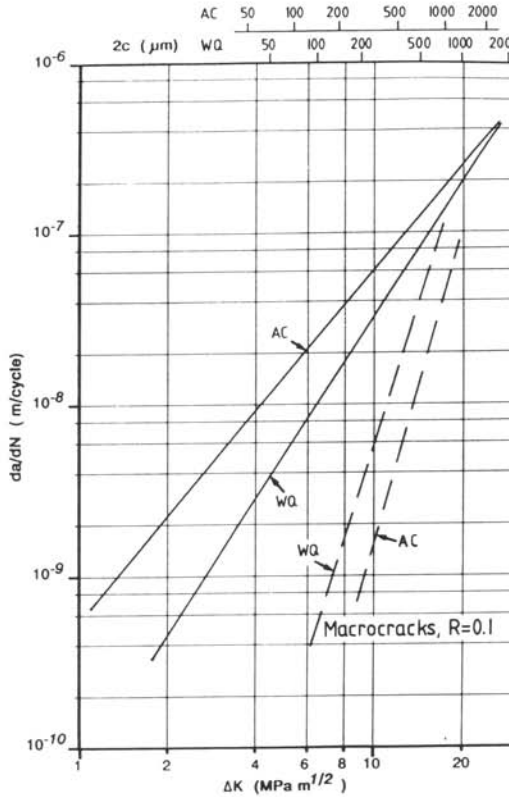


Fig. 40: Fatigue crack propagation of microcracks and macrocracks for different cooling rates of fully lamellar structures, Ti-6242.

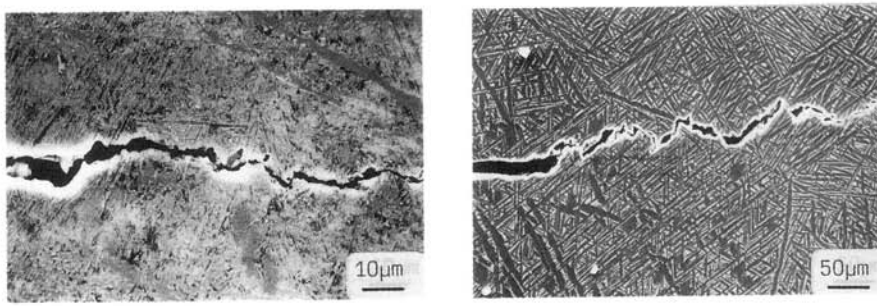


a) Fine lamellar b) Coarse lamellar

Fig. 41: Crack path in center of fracture toughness specimens, Ti-6242.

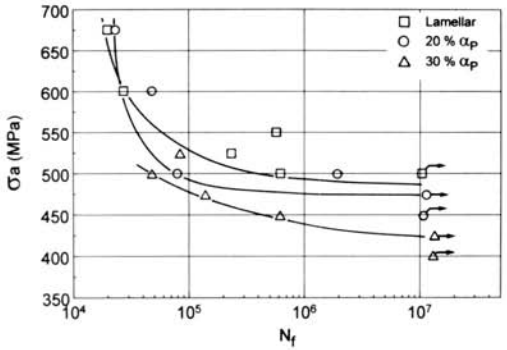


Fig. 42: HCF at RT, R = -1, IMI 834.

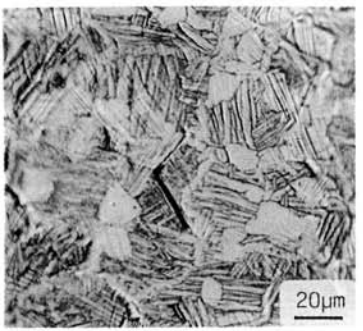


Fig. 43: Crack nucleation in lamellar region of bi-modal structure.

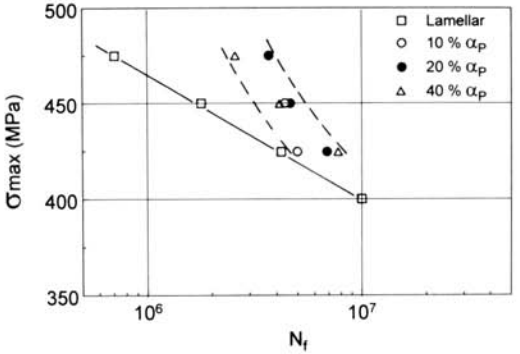


Fig. 44: HCF at 600°C, R = 0.1, IMI 834.

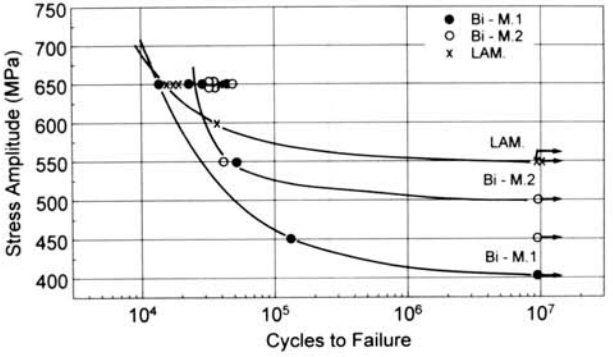


Fig. 45: HCF at RT, R = -1, IMI 834.

temperature (600 °C) the HCF strength is equal or higher for bi-modal microstructures as compared to the fully lamellar microstructure (Figure 44), demonstrating again that the alloy element partitioning effect is reduced at high temperatures.

The two bi-modal microstructures of the three different compressor disks (Figures 23b and c) might serve as an example for a constant alloy element partitioning effect ($\alpha_p$ volume fraction is constant) but with different $\alpha$ colony sizes. The comparison of the HCF strength in Figure 45 for the two bi-modal structures demonstrates the effect of $\alpha$ colony size on crack nucleation at low stress amplitudes. The large alloy element partitioning effect can be seen again by comparing the HCF strength values of the coarser bi-modal 1 structure and the fully lamellar structure. The LCF curves for these three different microstructures are shown in Figure 46. It can be seen that the lamellar microstructure exhibits the lowest LCF strength. This behavior was already indicated by the partial cross-over of the curves at high stress amplitudes in Figures 42 and 45. To separate the influence of crack nucleation and microcrack propagation on LCF life, the number of cycles until crack nucleation was investigated for the three microstructures (Table 6). It can be seen that the fatigue crack nucleation resistance at this relatively high stress amplitude was about the same for the lamellar and the coarser bi-modal 1 condition whereas the finer bi-modal 2 condition exhibited the highest crack nucleation resistance. Apparently, at high stress amplitudes the effect of $\alpha$ colony size (slip length) on crack nucleation resistance compensates (bi-modal 1) or overcompensates (bi-modal 2) the alloy element partitioning effect on crack nucleation resistance.

| Microstructure | $\sigma_a$ (MPa) | $N_i$ (Cycles) | 2c ($\mu$m) | $N_F$ (Cycles) |
|---|---|---|---|---|
| Lamellar | 650 | 9400 | 42 | 22600 |
| Bi-Modal 1 | 650 | 9500 | 44 | 31000 |
| Bi-Modal 2 | 650 | 12000 | 37 | 33800 |

Table 6: Crack initiation ($N_i$), corresponding crack size (2c), and cycles to fracture ($N_F$), RT, R = -1, 30 Hz, IMI 834

The microcrack propagation curves for the lamellar structure and the coarser bi-modal 1 structure are shown in Figure 47. It can be seen that the microcrack propagation rate was higher for the lamellar structure demonstrating the positive effect of the smaller $\alpha$ colony size of the bi-modal structure on microcrack propagation resistance. No significant difference in microcrack propagation behavior was found for the two bi-modal structures, which can be also deduced from the results shown in Table 6. Also shown in Figure 47 are the macrocrack propagation curves for these two microstructures exhibiting the anticipated opposite ranking due to the much rougher crack front profile of the lamellar structure overcompensating the positive effect of the higher ductility of the bi-modal structure.

For high temperature application, the creep resistance is a very important mechanical property in addition to fatigue resistance, especially in the primary creep region because

only small plastic creep strains are allowed for most aerospace structural parts. The plastic creep strain as a function of cooling rate is shown in Figure 48 for fully lamellar (cooling rate in step I) and bi-modal (cooling rate in step III) microstructures. It can be seen that the bi-modal microstructures exhibit a lower creep resistance than the fully lamellar structure over the whole cooling rate range investigated which can be explained by the alloy element partitioning effect. The increase in creep resistance in the low cooling rate region before the minimum in the curves in Figure 48 can be explained by the decreasing lamellae width with increasing cooling rate leading to increased strain hardening. The reason for the drastic decrease in creep resistance in the fast cooling regime after the minimum in the curves is still unclear. One possibility is that the annihilation process of dislocations at lamellae boundaries dominates over the strain hardening effect due to drastic increase in boundary density at fast cooling rates.

The effect of crystallographic texture on mechanical properties of ($\alpha$+$\beta$) titanium alloys thus far has a very limited use in structural parts. The dependence of HCF strength on texture type (Figure 22) and stress direction is shown in Figure 49 on the example of a fully equiaxed microstructure (see Figure 25), but the effects are similar for bi-modal microstructures. The HCF strength in vacuum (Figure 49a) is proportional to the yield stress, that means the transversal test direction (TD) being normal to the basal planes in B/T- and T-type of textures shows a higher HCF strength than the test direction being parallel to the rolling direction (RD). In aggressive environment (air tests or tests in 3.5% NaCl solution) the HCF strength shows a different dependence on texture (Figure 49b). The TD testing direction exhibits now lower HCF strength values than the respective tests in RD indicating that the basal planes are "embrittled" by hydrogen swept into the material by moving dislocations. A similar effect of the aggressive environment is found for fatigue crack propagation, as shown in Figure 50 again on the example of a fully equiaxed microstructure. In vacuum the dependence on texture is fairly weak (Figure 50a) because the ductility is fairly insensitive to texture and the contributions from crack front geometry and crack closure (Figure 36) are constant in this case. In aggressive environment (Figure 50b) the tests in TD direction show a much faster fatigue crack propagation rate as compared to tests in RD direction. Again, the basal planes are "embrittled" by hydrogen due to dislocation motion from the crack tip into the material but they are aligned unfavorably for crack propagation in RD tests (perpendicular to the crack propagation direction) and favorably in TD tests (parallel to the crack propagation plane).

Comparing the mechanical properties of fully equiaxed microstructures (Figure 25) with bi-modal microstructures (Figures 23b and c) in general terms, it is important that in case of a strong crystallographic texture the slip length in fully equiaxed microstructures can be much larger than the $\alpha$ grain size, reducing especially the resistance against fatigue crack nucleation (HCF strength). In other words, the volume fraction of $\alpha_p$ in bi-modal microstructures should be kept below about 50% to avoid extensive clustering of $\alpha_p$ grains.

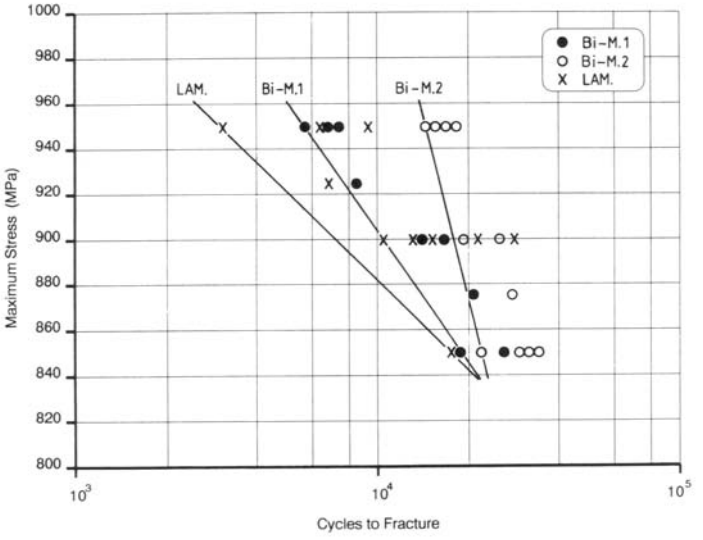


Fig. 46: LCF at RT, R = 0.1, IMI 834.

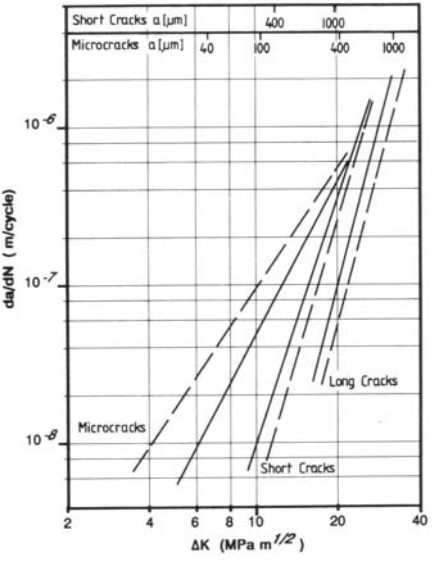


Fig. 47: Fatigue crack propagation, bi-modal 1 (solid lines) and lamellar (dashed lines), IMI 834.

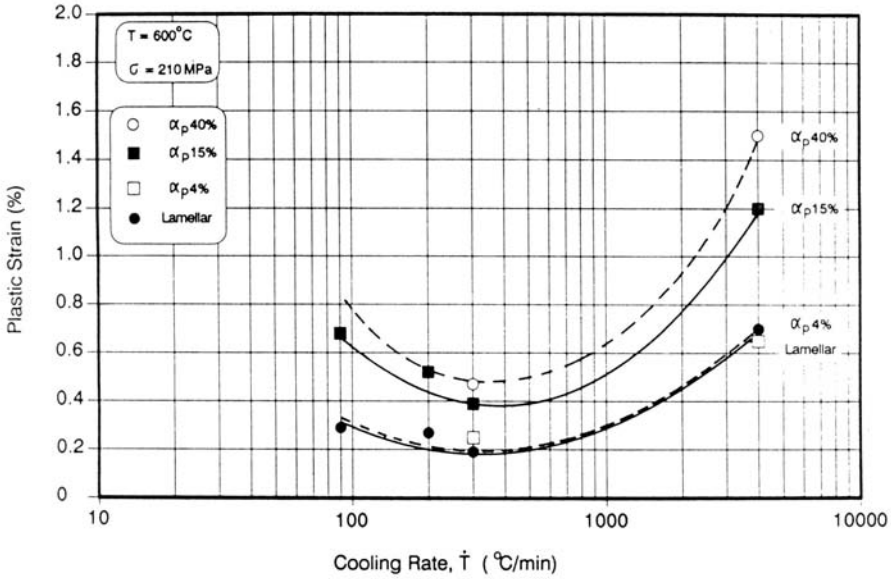


Fig. 48: Effect of cooling rate on creep strain, IMI 834.

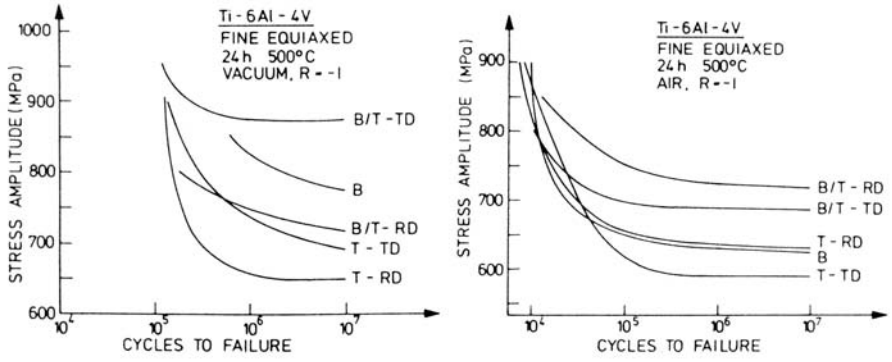


a) Vacuum b) Air

Fig. 49: Influence of texture and test direction on HCF strength, Ti-6Al-4V.

### 3.1.3 Bi-Lamellar Microstructures

Realizing that the large slip length in fully lamellar microstructures with large α colony sizes, resulting from relatively slow cooling from the homogenization temperature in this coarse grained material, has a disadvantageous effect on all mechanical properties except on macrocrack propagation (Figure 36), a so-called bi-lamellar microstructure was developed [29] in which the soft, single phase β "lamellae" (Figure 51a) are hardened by fine α plates (Figure 51b). In this way the effective slip length across the α colony width is reduced to the width of a single α lamellae. The easiest way to achieve this desired microstructure in a reproducible way seems to be the introduction of an intermediate annealing step X between step I and step IV in the normal processing route for fully lamellar structures (Figure 52). Important parameters of this step X are the correct choice of the annealing temperature and the cooling rate from this temperature (Figure 53). The mechanical properties of this bi-lamellar structure in comparison to the original lamellar structure are shown in Figure 54. It can be seen that the yield stress at room temperature as well as at 400 °C is increased drastically. Also, the resistance to fatigue crack nucleation (HCF strength) is increased, primarily due to the higher yield stress. The normally observed crack nucleation mechanism for fully lamellar microstructures in slip bands across the α colony width (Figure 55a) is changed to crack nucleation along α/β lamellae boundaries (Figure 55b), induced by slip parallel to the long dimension of the α lamellae. The improvement in creep resistance of the bi-lamellar structure as compared to the fully lamellar structure (Figure 54) can be explained by the reduction of creep strain in the β "lamellae". From Figure 36 it is anticipated that for the bi-lamellar structure also the resistance to microcrack propagation will be increased because the hardened β "lamellae" serve as strong obstacles to crack propagation. Figure 56 shows this effect, the microcrack propagation rate in the bi-lamellar structure being much slower than in the fully lamellar structure. It should be mentioned that the tensile ductility is not changed significantly by the change in microstructure from fully lamellar to bi-lamellar, but that the maximum in ductility in Figure 37 is reduced somewhat because of the stronger effect of continuous α-layers at β grain boundaries for bi-lamellar structures.

## 3.2 Beta Alloys

In this section on basic correlations between microstructure and mechanical properties of β alloys the discussion is focussed on comparing the three different microstructures described in Section 2.3. A more extensive describtion including other microstructural effects can be found in [30].

The yield stress of the β alloys depends primarily on the interparticle spacing (volume fraction and size) of the fine α platelets (Figure 29b) precipitated during the second aging step IVb (Figures 28 and 31). By omitting the first aging step IVa avoiding completely the formation of coarse α plates, the maximum volume fraction of fine α platelets is precipitated and yield stress values in excess of 1500 MPa can be reached

fairly easily in β alloys. Unfortunately, the tensile ductility in that highly aged condition tends to be close to zero. The other extreme would be to have only coarse α plates and no fine α platelets. In this case, the yield stress level would be around or below 1000 MPa. In between, any desired yield stress value can be easily obtained by chosing the appropriate temperature for the first aging step IVa determining in that way what volume fraction of α is left for precipitating as fine α platelets in step IVb. As pointed out already in Section 2.3, the tensile ductility is strongly affected by the presence of a continuous α layer at β grain boundaries (Figure 29a). The tensile properties of the three different microstructures discussed in Section 2.3 are shown in Table 7 on the example of the β alloy β-CEZ. The yield stress was adjusted to a constant level of about 1200 MPa for the three microstructures by keeping the heat treatment for step III (1 h 820 °C, cooling rate 100 °C/min) and step IV (8h 580 °C) constant. It can be seen that the lamellar (β annealed) condition exhibited the lowest ductility with about 4% tensile elongation. This can be explained by the large size of the equiaxed β grains (300-400μm) in combination with the continuous α layers along the β grain boundaries which are much softer than the age hardened matrix. These soft grain boundary layers result in a ductile "intergranular" failure at low overall macroscopic strains. The necklace microstructure exhibited a fairly high ductility in L-direction and a low ductility in ST-direction in accordance with the pancake shaped β grains (Figure 32). The tensile elongation value in ST-direction is somewhat higher (6%) compared to the lamellar structure (4%) because the continuous α layer is broken up in the necklace microstructure. The highest ductility was observed for the bi-modal structure primarily because of the small β grain size of about 40μm (Figure 30).

| Microstructure | $\sigma_{0.2}$ (MPa) | UTS (MPa) | Tens.El. (%) | RA (%) | $K_{Ic}$ (MPa $m^{1/2}$) |
|---|---|---|---|---|---|
| Lamellar | 1180 | 1280 | 4 | 10 | 52 |
| Necklace (L) | 1190 | 1275 | 10 | 16 | 68(T) |
| Necklace (ST) | 1185 | 1280 | 6 | 10 | 37(L) |
| Bi-modal | 1200 | 1275 | 13 | 34 | 37 |

Table 7: β-CEZ, tensile properties and fracture toughness values of the three different microstructures

For a discussion of the fracture toughness values (Table 7), the detailed crack front geometry should be taken into account, as described already in Section 3.1 (Figure 36). The fracture surfaces and the crack front profiles are shown in Figures 57 and 58. It can be seen already from the fracture surface that the geometry of the crack front in the region of unstable fracture was quite different for the different microstructures. In the lamellar condition (Figure 57a) the crack tried to follow the β grain boundaries as described already for the tensile specimens. In case of the necklace microstructure the crack also tried to follow the β grain boundaries. Due to the pancake grain shape of this microstructure (Figure 32) the fracture surface appearance is drastically different for

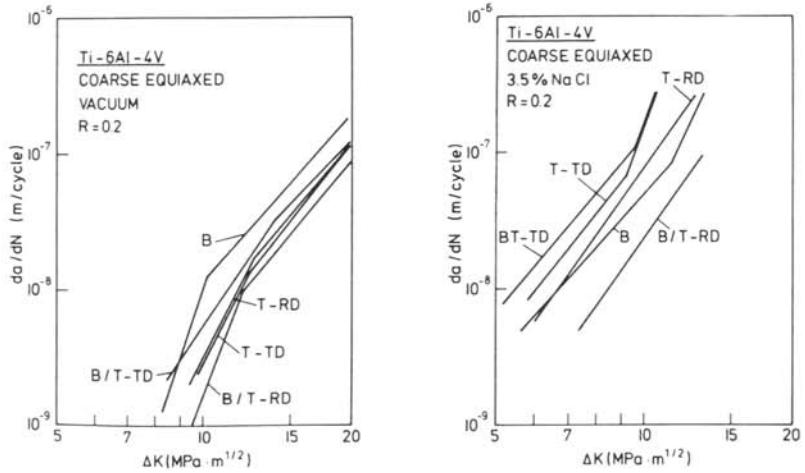


a) Vacuum b) 3.5% NaCl solution

Fig. 50: Influence of texture and test direction on fatigue crack propagation, Ti-6Al-4V.

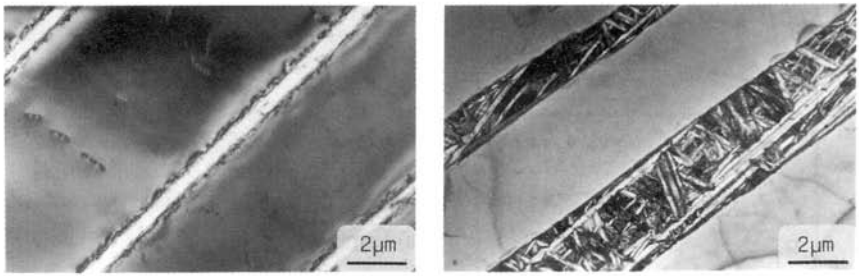


a) Lamellar b) Bi-lamellar

Fig. 51: Microstructure in β phase, TEM.

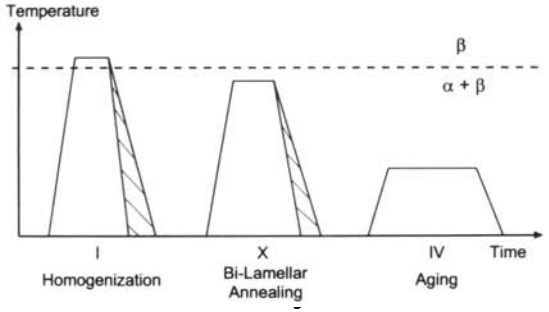


Fig. 52: Processing route for bi-lamellar microstructures (schematically).

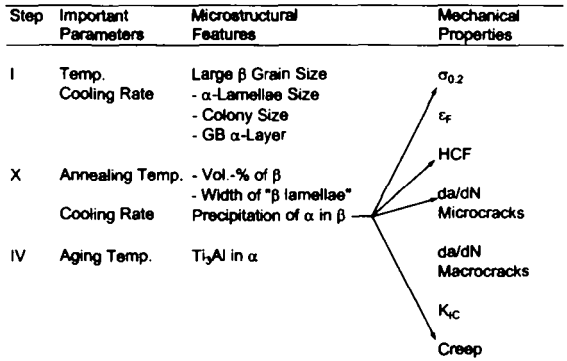


Fig. 53: Important processing parameters, resulting microstructural features, and major influences on mechanical properties (arrows) for bi-lamellar microstructures.

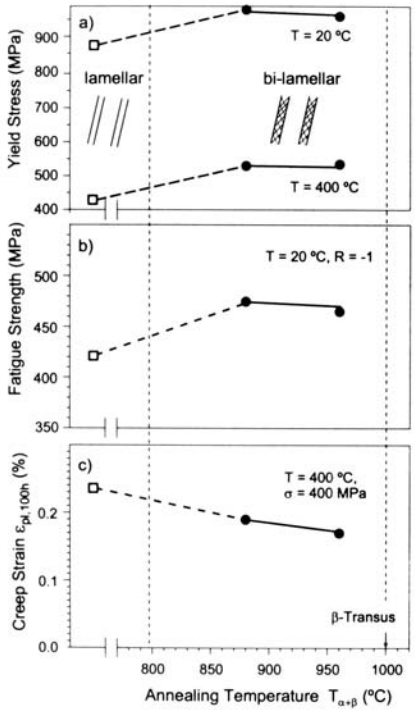


Fig. 54: Mechanical properties of lamellar and bi-lamellar microstructures, Ti-6Al-4V.

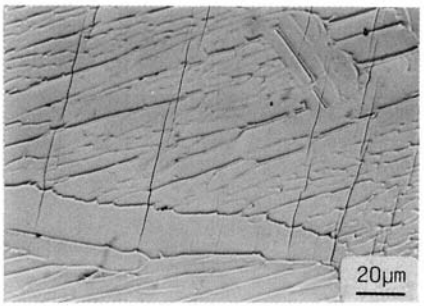


a) Lamellar

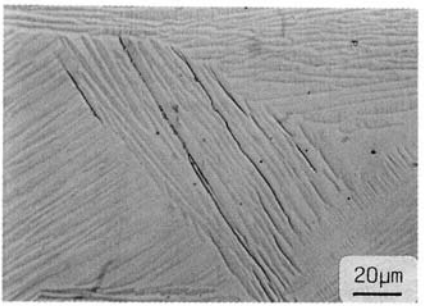


b) Bi-lamellar

Fig. 55: Fatigue crack nucleation mechanisms, Ti-6242.

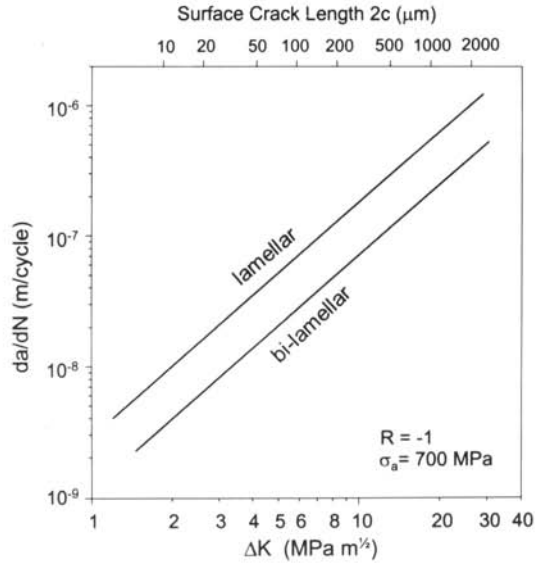


Fig. 56: Microcrack propagation curves for lamellar and bi-lamellar structures, Ti-6242.

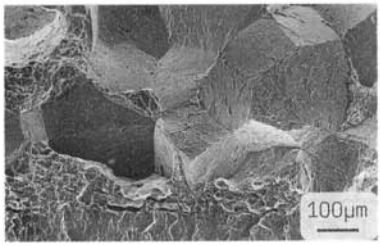


a) Lamellar


b) Necklace (L)

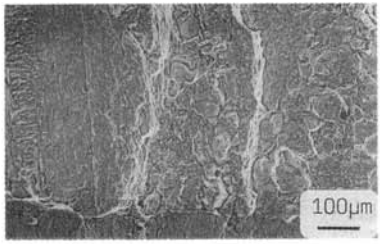


c) Necklace (ST)

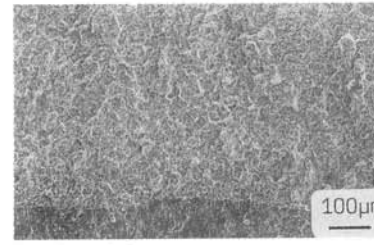


d) Bi-modal

Fig. 57: β-CEZ, fracture surfaces of $K_{Ic}$-specimens (macrocracks), SEM.


a) Lamellar ($K_{Ic}$ = 52 MPa $m^{1/2}$)

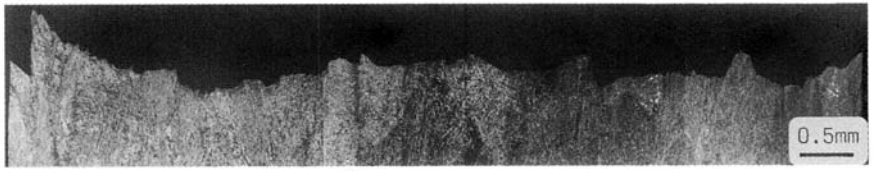


b) Necklace (L) ($K_{Ic}$ = 68 MPa $m^{1/2}$)

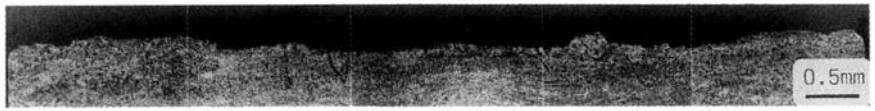


c) Necklace (ST) ($K_{Ic}$ = 37 MPa $m^{1/2}$)

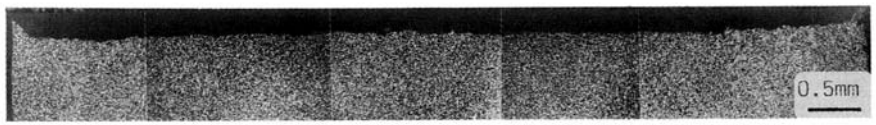


d) Bi-modal ($K_{Ic}$ = 37 MPa $m^{1/2}$)

Fig. 58: β-CEZ, crack front profiles of $K_{Ic}$-specimens (macrocracks), LM.

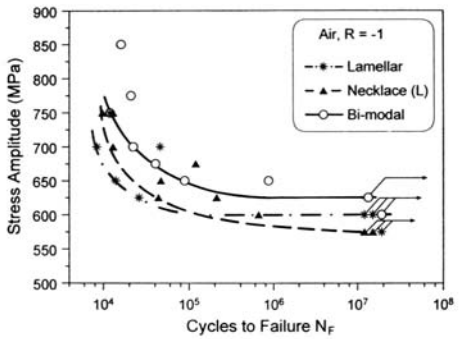


Fig. 59: S-N curves as a function of microstructure, β-CEZ.

testing in L-direction (Figure 57b) as compared to the ST-direction (Figure 57c). Since for the L-direction the flat surfaces of the pancake shaped grains are parallel to the stress direction (L) and parallel to the crack propagation direction (T), the fracture surface exhibited long and high steps often with deep secondary cracks (Figure 57b). For the ST-direction the flat surfaces of the pancake shaped grains are parallel to the crack plane and therefore the height of the steps is limited by the pancake thickness and the overall appearance of the fracture surface is very flat (Figure 57c). The fracture surface of the bi-modal condition (Figure 57d) is very flat due to the small β grain size. The difference in the geometry of the crack front between the different microstructures can be better seen by sections perpendicular to the crack propagation direction over the total width of the fracture toughness specimens revealing the crack front profiles (Figure 58). The crack front profiles for the bi-modal condition (Figure 58d) and for the necklace microstructure tested in ST-direction (Figure 58c) are very flat and the corresponding fracture toughness values are in both cases 37 MPa $m^{1/2}$ (Table 7). The crack front profiles for the lamellar condition (Figure 58a) and for the necklace microstructure tested in L-direction (Figure 58b) are both very rough with steps reaching a height of 500 μm. This crack front geometry is hindering crack propagation and the resulting fracture toughness values are 52 MPa $m^{1/2}$ for the lamellar structure and 68 MPa $m^{1/2}$ for the necklace (L) condition (Table 7). The difference in fracture toughness between these two conditions is obviously a result of the different angle of the steps with respect to the crack propagation direction which cannot be seen in the crack front profile pictures (Figure 58) but are clearly observed in the fracture surface micrographs (Figure 57).

The resistance against fatigue crack nucleation ($10^7$ cycles fatigue strength) is primarily determined by the yield stress with a value of about 0.5 for the ratio of HCF strength (R = -1) to yield stress. Figure 59 shows the S-N curves for the three different microstructures at a yield stress level of about 1200 MPa. It can be seen that the HCF strength values are close to 600 MPa with the tendency that the bi-modal microstructure had a slightly higher resistance against fatigue crack nucleation than the other two structures (lamellar and necklace). Also not much difference was found for the S-N curves of the two test directions (L and ST) for the necklace microstructure. The fatigue crack nucleation sites are shown in Figure 60. For the lamellar structure the cracks nucleate at the continuous α layers at β grain boundaries (Figure 60a), whereas for the other two microstructures the cracks nucleate at coarse α plates in the β matrix. The higher HCF strength of the bi-modal microstructure is then in agreement with the much smaller maximum length of α plates due to the small β grain size (Figure 60c) as compared to the necklace microstructure (Figure 60b). The crack propagation rates of these microcracks are shown in Figure 61 together with the propagation rates for macrocracks. It was found that the microcracks in the lamellar structure exhibited the fastest propagation rates as long as they propagated along the continuous α layer. After reaching the neighboring β grains they deviated from the continuous α layer and propagated through the matrix approaching the propagation curves for the other two microstructures and the curves for the macrocracks (Figure 61). The macrocracks in the

bi-modal microstructure exhibited the slowest propagation rates due to the small β grain size hindering propagation. For the macrocracks only transcrystalline crack propagation was observed even for the lamellar microstructure and the propagation curves are close togehter (Figure 61). The roughness parameter (Figure 36), although being fairly small in case of fatigue crack propagation in these β alloy microstructures, was found to be in agreement with the length of the coarse α plates explaining the ranking of the macrocrack curves in Figure 61.

To evaluate the maximum effect of the size of the α plates on fatigue crack propagation of macrocracks, two extreme microstructures were compared (Figures 62 and 63). For the fine lamellar structure (Figure 62) the first aging step IVa was omitted and only fine α platelets were present. For the coarse lamellar structure (Figure 63) the first aging step IVa was done in such a way that only coarse α plates were present in the microstructure and no α platelets were formed in step IVb. The resulting macrocrack propagation curves are shown in Figure 64. It can be seen that the maximum possible variation in the ΔK threshold region by varying the α plate structure in β alloys seems to be about 2 MPa $m^{1/2}$ explaining the insensitivity of fatigue crack propagation to microstructural variations for β alloys reported so often in the literature.

## 4. PROPERTIES AND APPLICATIONS

The choice of materials by a designer is a complex and sometimes not particularly systematic process. Factors that enter into the selection process are not only properties, which are well documented for titanium alloys in [11], but also prior experience, raw materials cost, fabricability, and other related factors. In high performance structural applications the density normalized strength, high temperature strength, creep resistance and other mechanical properties make titanium alloys a natural choice for many components. In the so-called commercial applications, that is for apparatus for the chemical and petrochemical processing industry, the choice of Ti alloys becomes less obvious. Titanium is well known for its corrosion resistance and general inert chemical behavior. This makes it an attractive material of construction in many aggressive environments. In these applications, titanium seldom is the only choice. Therefore, the competing materials such as stainless steel, some of the inconels and monels are also usually considered by the designer. Because titanium typically is more expensive, the life cycle costs of titanium, as determined by durability, becomes an important aspect of the final materials selection decision.

### 4.1 Alpha Titanium Alloys

Today millions of pounds of commercially pure and slightly alloyed titanium alloys are used annually in heat exchangers (both tube and plate type), liners for tanks, other chemical processing apparatus, and a variety of other applications in chemical and petrol-chemical industry. The vast majority of this titanium is unalloyed titanium or

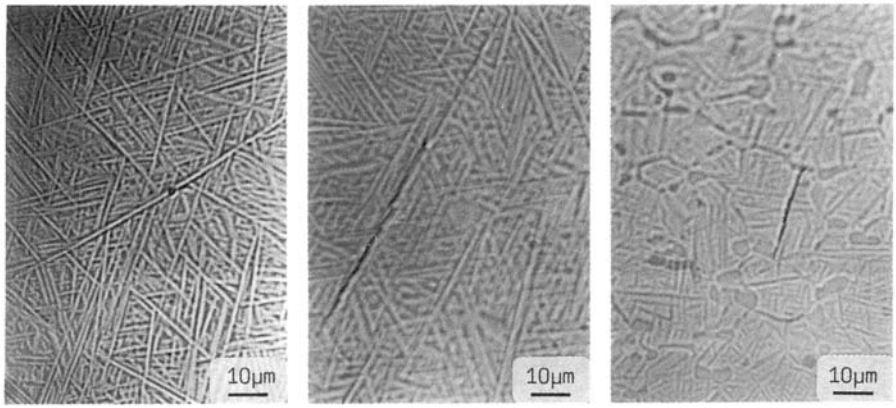


a) Lamellar structure b) Necklace structure (L) c) Bi-modal structure

Fig. 60: Fatigue crack initiation, LM, β-CEZ.

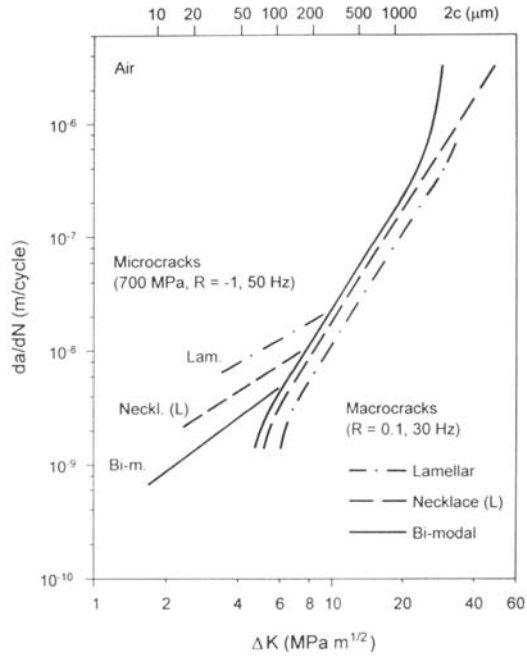


Fig. 61: da/dN-ΔK curves of micro- and macrocracks as a function of microstructure, β-CEZ.

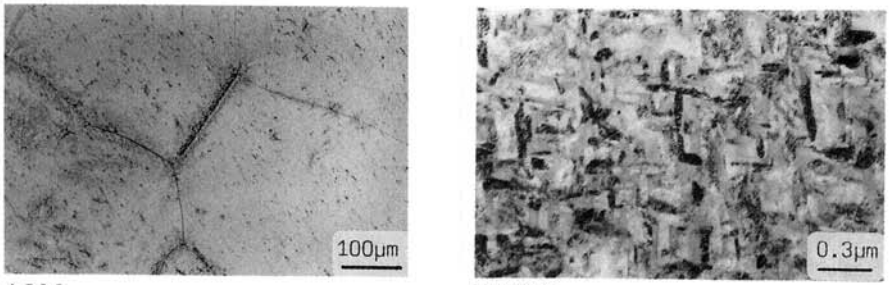


a) LM b) TEM

Fig. 62: Fine lamellar microstructure, β-CEZ.

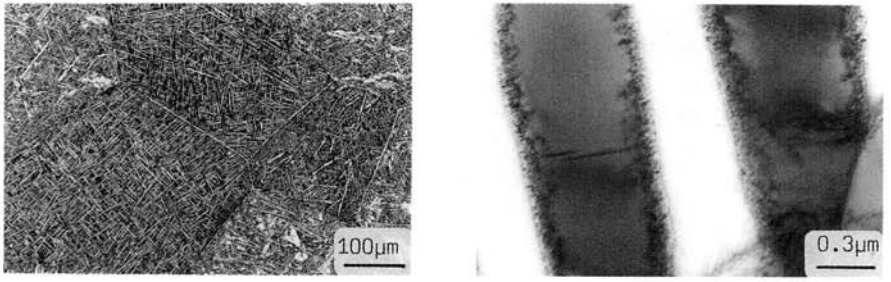


a) LM b) TEM

Fig. 63: Coarse lamellar microstructure, β-CEZ.

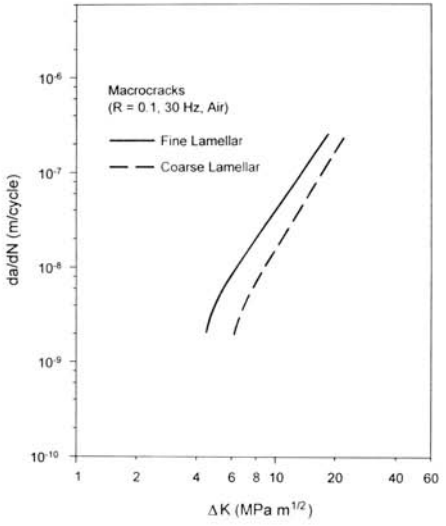


Fig. 64: da/dN-ΔK curves of fine and coarse lamellar microstructures, β-CEZ.

commercially pure (CP) as it is often called . CP Titanium is 98 % or more alpha phase, the remaining being iron stabilized beta phase. As has been described earlier (Section 1.6.1), oxygen is a potent α-phase solid solution strengthener. Thus the oxygen concentration in the alpha phase is the primary variable that determines its tensile properties, particularly strength. There are four common grades of CP titanium and these are designated in ASTM Specifications as grades 1 through 4. Table 8 shows the properties of these four grades of CP Titanium. From Table 8 it can be seen that the yield strength of grade 1 is less than half that of grade 4, while the yield strength of grades 2 and 3 lie in between these two extremes. This table also shows that the ductility of grade 4 is somewhat less than grade 1 but that the variation in ductility is substantially less than the variation in strength. Most applications for CP Titanium are not fatigue critical but, on occasion, a vibratory excitation can occur in a structure in a chemical plant due to pumps and other rotating machinery. In such cases, it is important to note that the crack nucleation stress is essentially proportional to the yield stress (see Figure 36) and the ratio of the fatigue strength (at $10^7$ cycles) to the yield stress is essentially constant with a value of ~0.73. Therefore, in applications where fatigue failure is possible due to vibratory excitation, it is advisable to use the highest possible yield strength (higher oxygen grades). That is, the highest ASTM grade of CP titanium that can be affordably fabricated. Small grain size also increases yield stress, so processing to obtain fine grains also is beneficial to fatigue strength.

| Alloy | E (GPa) | $\sigma_{0.2}$ (MPa) | UTS (MPa) | Elongation (%) | $\sigma_{10^7}$ (MPa) (R = -1) | $\sigma_{10^7}/\sigma_{0.2}$ |
|---|---|---|---|---|---|---|
| Grade 1 | 105 | 170 | 240 | 24 | - | - |
| Grade 2 | 105 | 275 | 345 | 20 | - | - |
| Grade 3 | 105 | 380 | 445 | 18 | 280 | 0.73 |
| Grade 4 | 105 | 480 | 550 | 15 | 350 | 0.73 |

Table 8: Typical mechanical properties of CP Titanium

One of the primarily attractive features of CP Titanium is that it is very fabricable because it is easy to weld using tungsten inert gas (TIG) techniques and is quite cold formable (Section 2.1). The major difficulty in cold forming CP Titanium is the occurrence of spring back due to the relatively low modulus and high yield stress. This results in large elastic strains compared to stainless steel. These elastic strains are relaxed after forming leading to a reverse elastic deflection. This can be accommodated in the forming or fabrication process design with experience but the degree of springback exhibited by CP Ti is distinctly larger than that of austenitic stainless steel which has low yield and high modulus. Thus experience and understanding of this point by the designer is very helpful.

The weldability of CP Ti is a critical requirement in nearly all fabrication plans. In addition, the excellent weldability of CP Ti makes the relatively low cost, automated

production of welded CP Ti tubing quite straightforward. It also facilitates further fabrication and assembly of large structures in the field using TIG welding techniques. Another issue that effects the decision regarding which grade of CP Titanium to use is the need (or lack thereof) to attach tubes to tube sheets in tube-type heat exchangers using technique known as roller expansion. Roller expansion uses a tapered rotary mandrel that plastically deforms or expands the tube, increasing its diameter until it interferes with the perimeter of the hole in the tube sheet, creating a seal between the heat exchanger tube and the tube sheet. There are several issues associated with successful roller expansion. One is adequate ductility to support the plastic strain imparted during the operation. Another is the force required to complete the operation, which is determined by the yield stress. Since roller expansion is a manual operation the latter point becomes a significant limitation as the size of the tubes and the tube wall thickness increases. At some point the required forces exceed the physical strength capability of many roller expander operators.

As described earlier in this chapter (Section 1.2), alpha titanium deforms in part both by slip and by mechanical twinning. The formability of CP Ti is aided by the occurrence of limited amounts of twinning (Section 2.1). The propensity for twinning is determined to a significant degree by the oxygen concentration of the alpha phase. Therefore, in applications where the yield strength is not critical and large plastic strains are required to allow forming of details, low or medium oxygen material is preferred. In some applications with very stringent formability requirements, the secondary effect of grain size on the propensity for twinning also can be beneficially utilized. That is, in special applications where very large plastic strains are required for fabrication, grades 1 or 2 have been successfully heat treated to increase the grain size and enhance the formability due to an increase in the amount of mechanical twinning. While this is an unusual circumstance, it is mentioned here to emphasize that the observations of mechanical twinning can be important technologically as well as scientifically.

## 4.2 Alpha + Beta Titanium Alloys for High Temperature Use

Alpha + beta titanium alloys are conveniently divided according to their strength and/or their application temperature regime. In this section high temperature alpha + beta Ti alloys (service temperature ≥325°C) will be discussed first. Today (in the western world at least) there are really only three high temperature titanium alloys in widespread use. These are: Ti-6-2-4-2, IMI-685, and IMI-834. The tensile and fracture toughness properties of these three alloys are shown in Table 9. By far, the largest application of these alloys is in the compressor section of aircraft engines. These alloys are attractive for this application because they have reasonably good density corrected strength and very good density corrected creep resistance. Processing of high temperature titanium alloys such as Ti-6-2-4-2 or IMI-685 has a major influence on properties, both in terms of strength and in terms of toughness and creep resistance (see Sections 2.2 and 3.1). Since these alloys are almost exclusively used as forgings the processing is easier to control

compared to sheet rolling.

| Alloy | E (GPa) | $\sigma_{0.2}$ (MPa) | UTS (MPa) | Elongation (%) | $K_{Ic}$ (MPa $m^{1/2}$) | $T_{max}$ (°C) |
|---|---|---|---|---|---|---|
| Ti-6242 | 114 | 940 | 980 | 16 | 55 | 500 |
| IMI 685 | 120 | 910 | 1020 | 11 | 65 | 500 |
| IMI 834 | 120 | 950 | 1050 | 12 | 45 | 550 |

Table 9: Typical mechanical properties and maximum usage temperature ($T_{max}$) of high temperature $\alpha+\beta$ Titanium Alloys

All modern aircraft engines have portions of the compressor that operate in the temperature range 325°C to about 575°C and have high temperature titanium (one of the alloys shown in Table 9) for the highly stressed rotors. These rotors are fabricated by forging and welding; an example of a rotor structure is shown in Figure 65. High temperature titanium alloys are not particularly strong but have excellent creep resistance. The yield and tensile strengths of Ti-6-2-4-2 for example, are significantly less than higher strength alloys such as Ti-17 used at lower temperatures. This is shown in Figures 66 and 67. Because titanium alloys have approximately 50 percent lower density than nickel base alloys they are very competitive at intermediate temperature ranges for weight sensitive, creep resistant applications such as rotors in gas turbine engines (Figures 68 and 69). The creep strength of high temperature titanium alloys like Ti-6-2-4-2 is substantially better than that of the lower temperature, higher strength alloys such as Ti-17. This is shown in Figure 70. All the high temperature titanium alloys, shown in Table 9 contain small concentrations (less than 0.3 weight percent) silicon. This silicon largely is responsible for the improvement in creep strength. The creep behavior of titanium alloys is not as well understood as that of nickel base alloys, but the silicon effects are quite well characterized and have been reproducibly demonstrated. There also are microstructure effects with regard to the creep strength of titanium alloys. Beta processed or lamellae structures have considerably better creep of strength than equiaxed or bi-modal microstructures (Figure 48). Additionally, high temperature titanium alloys have a relatively small volume fraction of beta phase. The improved creep strength of high temperature titanium alloys therefore is derived from some combination of silicon additions, the lamellae structure, and the relatively low fraction of beta phase. Since Ti rotor alloys also are fatigue limited, a balance between creep and fatigue can be achieved by processing (see Section 2.2.1) to produce a bi-modal microstructure with a low (10-15 vol. %) primary alpha phase. The addition of Carbon to IMI 834 makes this microstructure more reproducibly attainable during solution heat treatment.

The most comprehensive study of silicon effects in titanium alloys has been done by Flower, Swann, and West [31]. They showed that zirconium additions reduce the solubility for silicon and thus the addition of up to four or five weight percent of zirconium in high temperature titanium alloys is standard because it is helpful in

improving and controlling creep strength. Silicon additions in excess of about 0.1 weight percent lead to the precipitation of titanium silicides ($Ti_5Si_3$). These silicides have a complex chemistry and have zirconium substituted for some of the titanium and are really $(Ti,Zr)_5Si_3$. An example of titanium silicides in a high temperature titanium alloy is shown in the electron micrograph, Figure 71. The presence of these silicides do not provide for creep strengthening via dispersion strengthening, but they help stabilize the alpha/beta boundaries and also reduce boundary sliding. There also is silicon in solid solution which tends to provide dynamic strain aging and this effect contributes to the improved creep strength of Si bearing high temperature Ti alloys.

### 4.3 High Strength Alpha + Beta Titanium Alloys

High strength alpha + beta titanium alloys range in strength from 800 to 1250 MPa. The factors which effect the strength of these alloys are processing, heat treatment, and initial alloy composition, all of which affect and control the development of microstructure in the final use condition (see Section 2.2). Six of the most commonly used alloys in the western world are shown in Table 10. Alloys in the lower strength ranges of this general class are often used in the mill annealed condition. Mill Annealed Ti-6Al-4V is typically alpha + beta hot rolled and given a short stabilization heat treatment at ~700 °C, mainly for stress relief. This is represented by steps II and IV of Figure 19. The benefit of using alloys in this condition is cost and the minimal residual stress compared to that which can be imparted during heat treatment. Residual stresses in the heat treated condition pose significant challenges during machining of forgings due to part movement and the resultant difficulty in meeting final dimensional tolerances. Nevertheless, the structural efficiency benefits gained from higher strength levels obtained by heat treating alloys such as Ti-6-2-4-6 and Ti-17 are so great that heat treated versions of these alloys are used commonly today. Also, a significant effort has been invested in learning how to minimize residual stresses and in dealing with machining distortion.

| Alloy | E (GPa) | $\sigma_{0.2}$ (MPa) | UTS (MPa) | Elongation (%) | $K_{Ic}$ (MPa $m^{1/2}$) | $T_{max}$ (°C) |
|---|---|---|---|---|---|---|
| Ti-17 | 114 | 1100 | 1170 | 11 | 65 | 400 |
| Ti-6242 | 120 | 1050 | 1200 | 7 | 55 | 400 |
| Ti-6-22-22 | 114 | 1090 | 1200 | 15 | 65 | 350 |
| Ti-8-1-1 | 120 | 930 | 1000 | 10 | 52 | 300 |
| Ti-6-4 | 115 | 950 | 1040 | 14 | 60 | 300 |
| Ti-6-4 ELI | 113 | 900 | 970 | 16 | 90 | 300 |
| IMI 550 | 115 | 1020 | 1130 | 12 | 60 | 400 |

Table 10: Typical mechanical properties and maximum usage temperature ($T_{max}$) of high strength $\alpha+\beta$ Titanium Alloys.

Fig. 65: Multiple stage Titanium compressor rotor (Ti-6242) used in an aero engine.

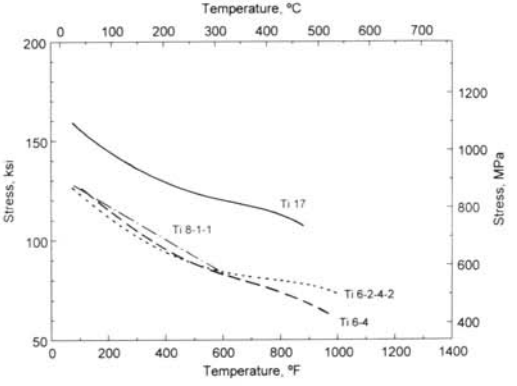


Fig. 66: Yield strength of four Ti-alloys as a function of temperature.

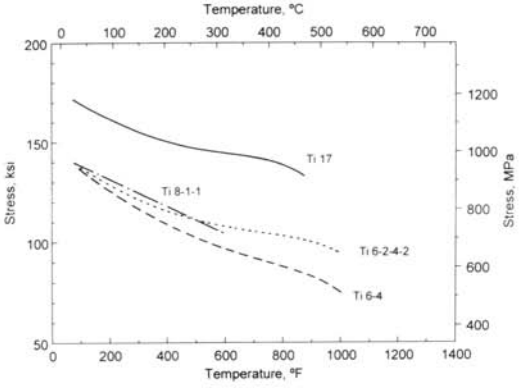


Fig. 67: Ultimate tensile strength of four Ti-alloys as as function of temperature.

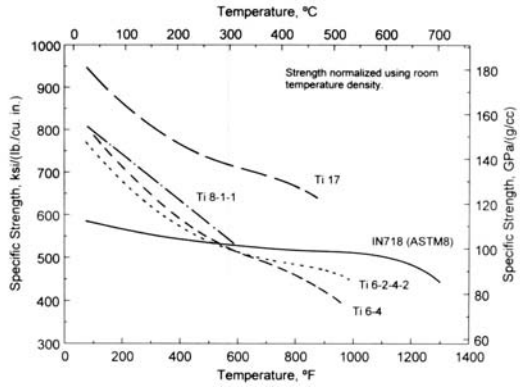


Fig. 68: Yield strength of four Ti-alloys and a Nickel base alloy, normalized for density.

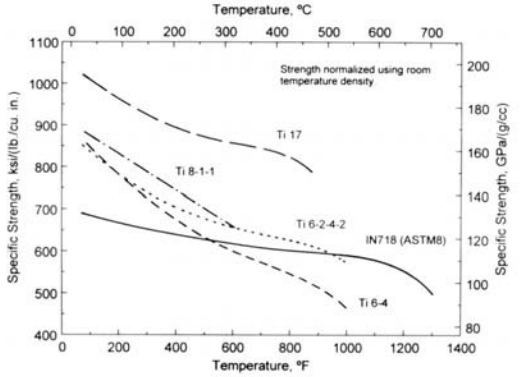


Fig. 69: Ultimate tensile strength, normalized for density.

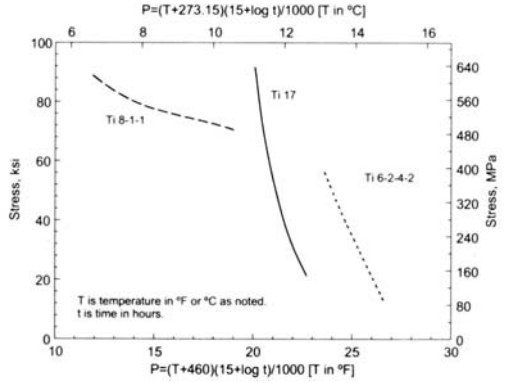


Fig. 70: Creep strength (0.2% plastic strain) versus Larson-Miller Parameter (P).

Tensile properties are often the first consideration in selecting an alloy for a structural application. In aircraft engines the primary uses of these alloys in wrought form (i.e. not cast) are for fan and low pressure ($T \leq 400$ °C) compressor rotors. In these components, other properties such as fatigue strength, crack growth resistance, and fracture toughness also are very important. The ductility and toughness ranges typical of these six alloys also are shown in Table 10. The fatigue properties of these alloys are shown in Figure 72. From this figure it can be seen that, in the high cycle fatigue regime ($10^6$ or greater cycles to failure), the fatigue strength scales with yield strength which dominates the fatigue performance. This is why in Figure 71 the curve for Ti-17 has a different shape than those for Ti-8-1-1 or Ti-6-2-4-2. There is a more detailed discussion of this point in Section 3.1. Today, where damage tolerant design is becoming increasingly important the fatigue crack growth behavior of titanium alloys is becoming the focus of considerably greater attention. Because titanium alloys can be microstructurally tailored with constant strength to optimize one of the various second tier mechanical properties such as ductility, toughness, and fatigue crack growth, this class of alloys is particularly interesting. Figure 73 shows the fatigue crack growth characteristics of three of the titanium alloys shown in Table 10. In this figure Ti-17 has relatively poor fatigue characteristics at low stress intensities but has better crack growth characteristics at higher stress intensities. At least a portion of Ti-17 fatigue behavior is dominated by the finer scale of the Widmanstatten structure. This structure is unusual in $\alpha+\beta$ Ti alloys, most of which exhibit a colony structure. The composition of Ti-17 leads to a low $\beta$ transus which promotes the basket-waeve or Widmanstatten structure during cooling. This is consistent with the relative rankings of the yield stresses of these three alloys (see the discussion in Section 3.1 and refer to Figures 40 and 47).

The typical applications for high strength low temperature alpha + beta titanium alloys include tanks for missiles and rockets, heavily loaded parts for aircraft, and heavily loaded parts for aircraft engines. Rocket engines have tanks that hold cryogenic fluids (fuel and oxidizer) and therefore operate in the 100 K range. For these applications, a special grade of Ti-6Al-4V called ELI grade (extra low interstitials) is used. The room temperature strength of this grade is lower as shown in Table 10, but at the service temperature it is about the same as that of standard grade Ti-6Al-4V at room temperature. A high volume, more traditional use for high strength titanium alloys are for rotating parts such as front rotors in aircraft engines, fan disks, low pressure compressor disks. An example of a Ti-17 fan disk is shown in Figure 74. A typical aircraft structural part such as a Ti-6Al-4V bulk head forging from high strength titanium is shown in Figure 75. Today, aircraft structural parts are largely made from Ti-6Al-4V because it has better structural efficiency and durability than Al alloys. Table 10 shows other alloys that could be even more structurally efficient, but cost and lack of experience in designing with these other alloys has led to the continued principal use of Ti-6Al-4V.

The maximum use temperature for this class of alloys is about 400°C as shown in Table 10. The reason for this limitation is not yield strength or tensile strength but rather creep behavior. Figure 70 compares the creep strength of Ti-17, for example, to the

higher creep strength, lower tensile strength alloy Ti-6-2-4-2. Contrasting this creep behavior to tensile behavior shown in Figures 66 and 67 allows this point to be understood more clearly.

There are other applications, but from a volume standpoint these have been relatively small. Alloys such as Ti-6-4 are also becoming popular for sporting goods applications and a current "fad" is the use of Ti-6-4 for the heads of drivers in golf clubs. These club heads have a complex array of internal stiffening ribs and are most economically made by investment casting. A picture of a cast golf club head is shown in Figure 76. In 1997 ~ 9 million pounds of Ti was consumed by golf clubs, which is ~ 5 - 10% of the world production. Such "fads" disrupt the long term supply and demand and make capacity planning very difficult for the producers.

The high yield strength and relatively low modulus of titanium alloys is a complication when considering formability as was discussed in the section on alpha (commercially pure) titanium alloys (Section 4.1). This same characteristic can be a benefit in other applications. For example, high yield stress and relatively low modulus allows very large elastic deflections at relatively low stresses, which can help minimize the susceptibility to fatigue failure in deflection dominated applications. One such application is the fixture that attaches the point of emergence of oil from the ocean floor in an offshore oil well to the pipe that brings the oil to the platform on the surface, (Figure 77). This fixture is sometimes called a "Christmas tree". In rough seas the platform and the pipe move to and fro as it receives the oil from the pipe, but, obviously, the opposite end of the pipe and the Christmas tree are fixed on the ocean floor. As a result there can be significant deflections in the pipes and the fixture on the ocean floor. Alloys such as Ti-6-4 are very useful in such applications because they have relatively high yield strength combined with a relatively low modulus and are capable of undergoing large elastic deflections without exceeding the yield stress. These alloys also are inert in salt water and this combination of characteristics makes them attractive for this application. These fixtures also are very large so the relatively low density of titanium also is helpful because it makes them easier to transport and to move into position to be lowered to the bottom of the ocean.

Another emerging application for high strength alpha + beta alloys also is related to their strength, modulus and their chemical inertness is medical implant applications. Today, titanium alloys (predominantly Ti-6Al-4V) are rapidly replacing cobalt based alloys because of a lower modulus and chemically inertness. The modulus of bone, for example, is less than 60 GPa. Thus titanium alloys with moduli on the order of 100 to 115 GPa are much more attractive than cobalt alloys whose modulus is greater than 200 GPa. Artificial hip implants in particular have become a popular application for titanium. While titanium is chemically inert, there is an on-going concern about both aluminum and vanadium in the human body, even in very small concentrations. As a result, new alloys (e.g., Ti-5Al-2.5Fe) are under development which contain either low or zero concentrations of aluminum and vanadium in order to achieve improved bio-compatibility. The qualification of these new allows is a long and arduous process

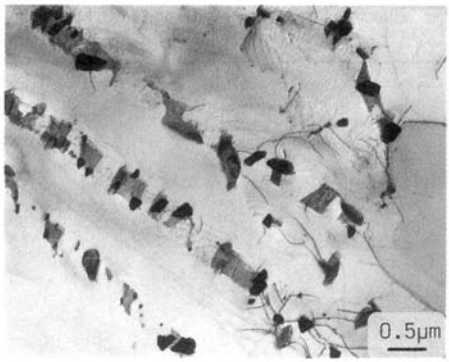


Fig. 71: Electron micrograph showing (Ti, $Zr)_5Si_3$ precipitates in IMI 834.

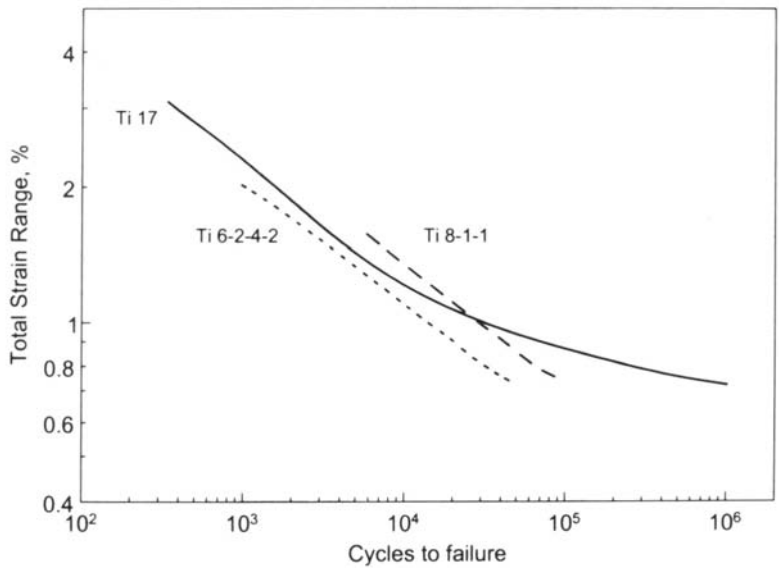


Fig. 72: Fatigue behavior of three Ti-alloys at room temperature (R = 0).

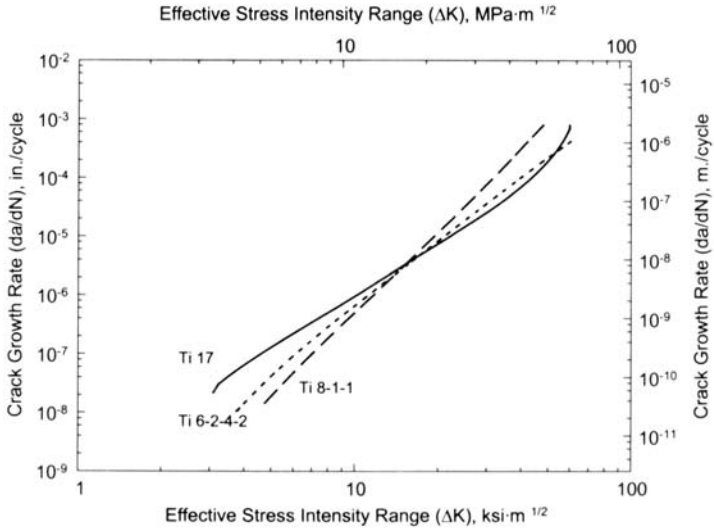


Fig. 73: Fatigue crack growth behavior of three Ti-alloys at room temperature (R = 0).

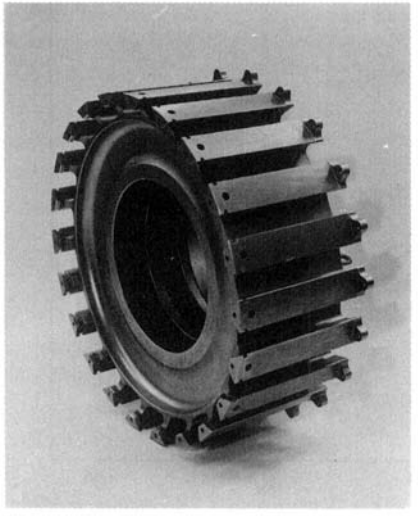

Fig. 74: Photo of a large Ti-17 fan disk forging for an aero engine.

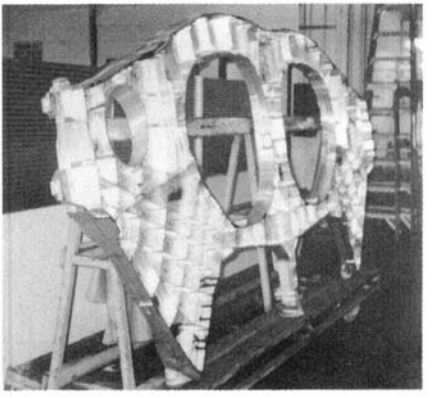

Fig. 75: Photo of a large Ti-6Al-4V aircraft structural forging (courtesey Laddish Corp.).

dominated by the Food and Drug Administration in the US and by similar regulatory agencies in other countries. The point here is that titanium alloys of one type or another have attractive characteristics for bio-medical applications in particular surgical implants, and that special bio-medical alloys are being developed.

Two near net shape fabrication methods for high strength titanium alloys have become important in the last five to ten years, investment casting and superplastic forming. Both of these have been shown to be cost effective methods of producing titanium components with complex geometries at a relatively low cost. Today titanium investment castings are used for a wide variety of applications both in aircraft and in aircraft engines. For example the hub of the front frame of a 747 class aircraft engine is a one piece Ti-6-4 casting with cast Ti-6-4 struts welded around the outboard perimeter. This casting is substantially larger than 1.5 meters in diameter and weighs approximately 250 kg. It also has substantial complexity and contains many detailed cast-in features, yet it is used in the as-cast and chem-milled condition. The extent of application of titanium structural castings continues to grow, due in part to the continuous improvement in shape making capability and dimensioned tolerance control that the investment casting industry has been able to achieve. Figure 78 shows a photograph of such large structural castings. A limiting feature of Ti structural castings today is the presence, on the as-cast article, of a thin layer of reaction product formed during interaction between the mold and the molten titanium metal. This reaction leads to a local oxygen enrichment and thin, nearly continuous layer of oxygen stabilized alpha phase at the surface, this layer is known as alpha case. Oxygen stabilized alpha phase can be hard and brittle, therefore the alpha case must be removed by chemical milling. Another limitation is porosity in the as-cast condition. This can be eliminated by a hot isostatic pressing (HIP) treatment. Ti structural castings are therefore given a HIP treatment and chemical milled prior to placing them into service. Cast Ti-6Al-4V has a relatively coarse, fully lamellar microstructure (see Figure 55). The ability to tailor the microstructure and properties of Ti castings is quite limited, maybe with the exception of creating a bi-lamellar microstructure as described in Section 3.1.3. However, even in a non-optimum condition Ti-6Al-4V castings are economically very attractive when compared to fabrications made from wrought products.

The other fabrication technique which has become popular is super plastic forming and diffusion bonding of titanium alloys. This fabrication process utilizes alpha + beta processed titanium alloy sheet as the input material and permits the fabrication of very complicated shapes. Alpha + beta titanium alloy sheet products tend to have a very fine (~10-15 μm diameter alpha grain size) microstructure (see Section 2.2.1). This microstructure is naturally superplastic and therefore allows the fabrication of very complicated shapes with a forming method that uses a single die and low pressure gas at temperatures of ~925° C. Superplasticity is the result of a strong strain rate sensitivity of the flow stress which allows large plastic strains to be achieved without plastic instability or fracture. Because the Ti alloy sheet is super plastic at these temperatures, it can literally be "blown" into the die cavity and exhibits essentially no spring back because the

elastic strains are very small. Titanium also has the characteristic of an increasing solubility for oxygen with increasing temperature. This characteristic causes the ever-present thin oxide on the surface of titanium to be dissolved by the base metal when heated above ~600°C (see Section 1.7.2), creating (in the absence of additional oxygen) a pristine surface. When two sheets of titanium are placed in intimate contact with one another and heated to ~600°C (or greater), the oxides on their surfaces dissolve and the two surfaces bond together almost perfectly. This phenomenon is known as diffusion bonding. Today, diffusion bonding is used in combination with super plastic forming to create very complicated and selectively reinforced shapes. That is, strips or pieces of titanium can be placed in the super plastic forming die and the sheet which is being super plastically formed then bonds to these strips when contact is made during the super plastic forming or deformation process. This creates the capability for making double walled structures and selectively reinforced structures which would be extremely expensive to produce by machining from forgings. One example is the manifold used in an aero engine as shown in Figure 79. Today, super plastic forming and diffusion bonding has been shown to be technically feasible but only limited numbers of components have been made by these techniques for real products, principally because of cost.

### 4.4 Beta Titanium Alloys

Beta titanium alloys, as discussed previously, are the most highly alloyed version of conventional titanium alloys. Beta alloys are attractive for heavy section applications because they can be heat treated to develop high strengths in very thick sections. Beta alloys also are easier to produce as sheet products, making them attractive for fabricated sheet structures. The advantages of beta alloys ,in principle, have been recognized for many years and there are older beta alloys that have been extensively used for applications such as the SR71 ("Blackbird") Supersonic Military Airplane. Because service temperatures during flight exceeded the capability of Al alloys, the skin and much of the structure of this airplane were made from one of the first production scale beta alloys known as B120VCA. The composition of this alloy is titanium plus 13% Vanadium, 11% Chromium, 3% Aluminum (Ti-13-11-3). This alloy was selected in the early '60's because it was easy to fabricate into sheet for use as the skin of the Blackbird. It has been described in earlier sections of this chapter that chromium is a eutectoid former in titanium alloys. One of the difficulties with B120VCA was that after long time, high temperature (>300°C) service exposure, the compound $TiCr_2$ precipitated and led to a dramatic loss of ductility. Moreover, alloys containing high concentration of the eutectoid forming alloying elements, such as iron, chromium, manganese, nickel, or cobalt, also have low melting eutectics which lead to troublesome freezing segregation during melting and solidification of commercial sized heats, where the solidification rates are slow. For these reasons, the newer beta titanium alloys have some, but much lower concentrations, of the eutectoid formers such as iron and chromium. Today, there are

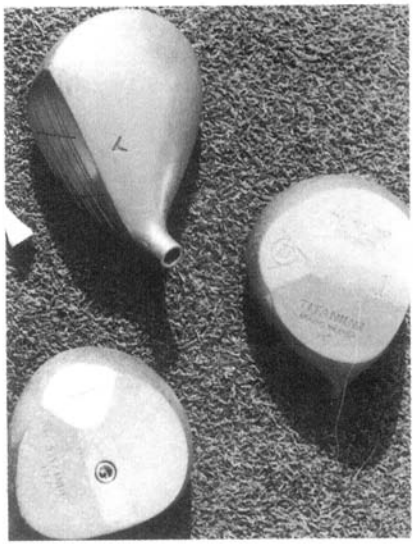

Fig. 76: Photo of an investment cast Ti-6Al-4V golf club head (courtesey Neil Paton, Howmet Corp.).

Fig. 77: Photo of Ti-6Al-4V taper stress joints used in an off-shore oil platform (courtesey RMI Corp.).

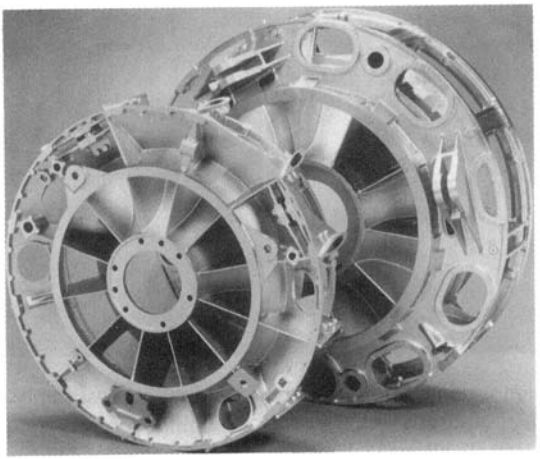

Fig. 78: Photo of large Ti-6Al-4V structural castings; fan frame hubs used in aero engines.

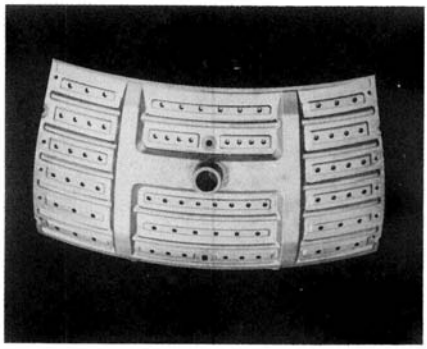

Fig. 79: Photo of a superplastically formed and diffusion bonded hot gas manifold (Ti-6Al-4V) used in an aero engine.

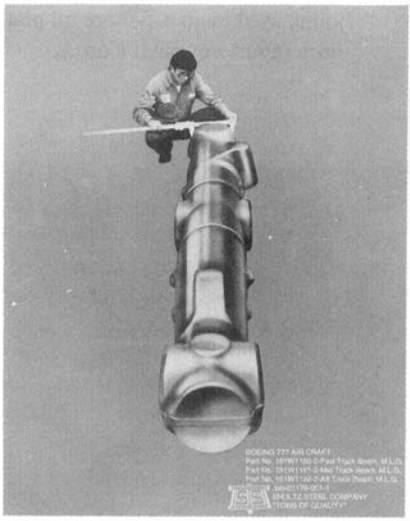

a) Rough truck beam forging

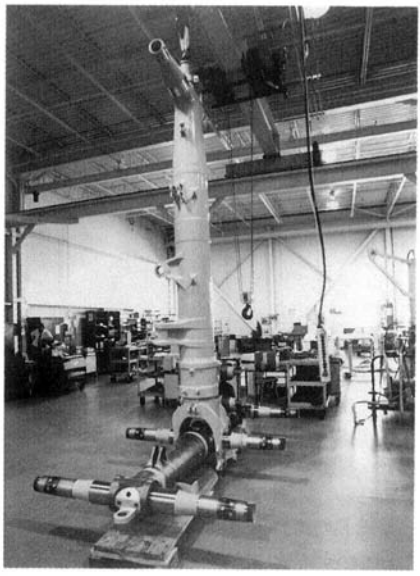

b) Landing gear assembly containing machined forging

Fig. 80: Photo of Beta Ti-alloy (Ti-10-2-3) forging for Boeing 777 landing gear (courtesey Rod Boyer, Boeing).

essentially only a few beta alloys that have commercial status. Some of these alloys together with their nominal properties are shown in Table 11. Among these, the most widely used is Ti-10V-2Fe-3Al (Ti-10-2-3) followed by Beta C (Ti-3-8-6-4-4) or Ti-15-3-3-3. Ti-10-2-3 and Beta C are typically used as forgings or extrusions, whereas Ti-15-3-3-3 is used as a sheet alloy. In fact, Ti-15-13-3-3 was developed as a replacement for the older B120VCA sheet alloy. Beta CEZ was developed in France and has very good strength properties. There also is a new alloy (Beta 21S) which is attractive because it has superior hot resistance to hydraulic fluid in aircraft. Table 11 shows that the strength levels of beta alloys can be significantly higher than those of the high strength alpha + beta alloys such as Ti-17 or Ti-6-2-4-6. The issue for highly loaded structures however is balancing strength and toughness, as described in Section 3.2. As a result, some of the strength capability of beta alloys can only be used in very restrictive applications such as springs, which will be described later. As mentioned earlier, crack growth behavior of titanium alloys is also becoming increasingly important. Because of the fine microstructural scale of beta alloys (which allows the high strength levels to be developed) beta alloys tend to not have particularly attractive fatigue crack growth rate characteristics, as described in Section 3.2 and illustrated in Figures 61 and 64. They do have good fatigue strengths (see Figure 59), which would be expected based on their high yield strength levels. Beta alloys can be processed and heat treated to exhibit a variety of microstructures (Section 2.3) and, as a result, allow significant tailoring of their properties.

| Alloy | E (GPa) | $\sigma_{0.2}$ (MPa) | UTS (MPa) | Elongation (%) | $K_{Ic}$ (MPa $m^{1/2}$) |
|---|---|---|---|---|---|
| Beta C | 114 | 1200 | 1260 | 8 | 48 |
| Ti-10-2-3 | 103 | 1155 | 1290 | 7 | 45 |
| β-CEZ | 120 | 1200 | 1280 | 11 | 45 |
| Ti-15-3 | 104 | 1210 | 1330 | 8 | 43 |

Table 11: Typical mechanical properties of β Titanium Alloys

While applications of beta titanium alloys are growing, in reality, they are still relatively few. This is especially true when one considers the length of time that beta alloys have been available as a conceptual materials class. The SR71 has been out of production for many years and only recently have beta alloys been reintroduced into aircraft. The largest volume applications of beta alloys today are in heavy landing gear components for commercial airplanes, particularly those made by Boeing. In these applications, titanium replaces steel at a significant weight savings and reliability improvement because high strength steels are much more susceptible to hydrogen embrittlement and stress corrosion cracking. Landing gear structures are mainly ultimate strength and fracture toughness limited rather than fatigue crack growth limited and, therefore, this represents an ideal application for beta titanium alloys. Figures 80a and b show a rough forging and a finished landing gear for the Boeing 777. These forgings are

made from the Ti-10-2-3 alloy. The size of these forgings is substantial as can be seen in the Figure. Beta alloys also have relatively low flow stresses in the forging temperature range and this is an additional benefit of making these components from this class of alloy. Another benefit is the high strength and the ability to achieve these high strengths in relatively large or heavy sections.

Beta titanium alloys also have a significant tolerance for hydrogen, compared to alpha or alpha + beta alloys (see Section 1.7.3). This characteristic makes them attractive for use in aggressive environments. One example is for oil and gas applications, where the service environment contains significant concentrations of $H_2S$. These environments are often referred to as sour gas environments. Heavy wall Beta C tubing with diameters up to ~50 cm and wall thicknesses of 1 to 3 cm is now being used in sour gas petroleum production applications in a number of locations (Figure 81). Another environment driven application is tolerance to hydraulic fluid at high temperatures. Here, the relatively new alloy Beta-21S, mentioned earlier in this connection, is gaining acceptance. This application also is related to its superior hydrogen tolerance.

There are two remaining applications where the very high strength of beta alloys is attractive because they are not limited by the relatively low fracture toughness values of this class of alloys (see Section 3.2). These are springs and fasteners. Beta titanium alloy springs have extremely large elastic deflection capability because of the very high yield stress and even lower elastic modulus compared to high strength alpha + beta alloys. Coil springs are essentially loaded in torsion and therefore toughness is a minor consideration. Notched sensitivity is important, but the notched tensile strength of beta alloys is acceptable. In fasteners, many of which are loaded principally in shear (as opposed to tension), a similar situation pertains. Namely, alloys with very high strength can be used without being limited by the relatively low fracture toughness, since this is not a controlling factor in shear loaded applications. Secondly, the superior fabricability of beta alloys, especially in the solution treated condition, makes fabrication of articles such as springs and fasteners relatively easy and therefore more cost effective. That is, the forming operation can be done in the solution treated condition, followed by aging to obtain very high strength. Figure 82 shows some examples of beta titanium alloy springs used in Boeing aircraft.

### 4.5 Titanium Based Intermetallic Compounds

Intermetallic Compounds have long been recognized as having interesting high temperature properties but the low temperature brittleness has been a significant impediment to their applications. Compared to high temperature Ni base alloys, there are several titanium based intermetallics that are especially attractive because of their low density. These are Alpha 2, based on $Ti_3Al$ (having an ordered hexagonal $DO_{19}$ structure), Orthorhombic Alpha-2, based on $Ti_2AlNb$ ($Ti_3Al$ plus substantial quantities of niobium which distorts the hexagonal structure) and Gamma, based on TiAl (having an ordered face-centered tetragonal $L1_0$ structure). All of these materials are still

developmental in nature but, among the three, Gamma appears to be moving toward earliest, limited introduction in aircraft engines.

One of the reasons that application of Gamma can now be seriously considered is that a great deal of progress has been made in learning to design with materials with low ductility, such as titanium based intermetallics. Therefore, the low temperature brittleness currently is much less a barrier to introduction than it was when intermetallics were first seriously examined. Further, there has been a lot of work devoted to learning how to alloy the titanium based intermetallics to improve their ductility. Today, low ductility is probably a more accurate characterization of these materials than brittle. Today, it also is correct to say that design requirements for ductility have become somewhat less stringent and the ductility characteristics of the titanium based intermetallics compounds have improved. These two factors have converged to an acceptable middle ground, making introduction of them into products a more realistic possibility. Furthermore, Gamma TiAl shows increasing ductility with increasing temperature and, therefore, concerns of low ductility are further reduced because the intended applications always are for service temperatures in the 700 - 900°C range. Thus low temperature ductility is principally a limitation for non-standard operating events in aircraft engines such as cold, hard starts and for non-service, limited frequency events such as assembly in the manufacturing shops and re-assembly after maintenance. Limited ductility also is a concern during component manufacturing where operations such as straightening, machining, etc. are used. In the case of Gamma, preliminary indications are that these operations require additional care but are manageable.

### 4.5.1 Alpha-2 and Orthorhombic Alloys (~25 at% Al)

The nominal 25 at % Al class of titanium intermetallics includes both the Alpha-2 and the Orthorhombic alloys. These will be discussed together because the latter evolved from the former. The early versions of Alpha-2 were alloyed with niobium to improve the room temperature ductility and to impart a higher creep strength and to allow the structure to be controlled by heat treatment. It turns out that achieving significant improvements in these properties required niobium concentrations of ~10 or greater atom percent and addition of such large concentrations of a heavy alloying elements such as niobium to Alpha-2 significantly increases the density of the material and simultaneously reduces the modulus. Both of these property changes make the material less attractive. Furthermore, niobium is an expensive alloying element and therefore newer generations of these alloys became more expensive and a cost:benefit analyses for them also became less and less attractive. Finally, it was discovered that the Alpha-2 class of alloys showed a susceptibility to an environmentally induced ductility reduction over the temperature range 675 to 725° C. As a result, the Alpha-2 alloys have largely fallen into disfavor and work on them for production applications has virtually ceased.

During, the efforts to develop the Alpha-2 alloys it was discovered that higher concentrations (>15 at %) of niobium led to the formation of an ordered orthorhombic

phase. Alloys containing this phase exhibit significantly higher strength and better fracture toughness than the Alpha-2 alloys. The Orthorhombic alloys also have a lower susceptibility to the intermediate temperature environmental embrittlement that was a major drawback for Alpha-2. The Orthorhombic Alpha-2 alloys are still under development but are considered to hold promise for structural applications. One of the attractions of these alloys is that they seem to have comparable temperature capabilities to nickel or iron base alloys for casings in jet engines but have ~50% lower thermal expansion coefficient. An unresolved concern is the flammability question under high mass flow conditions typical of the compressor casing service environment. This issue is still being examined and discussed. The ordered Orthorhombic alloys can be given a solution heat treatment followed by aging to obtain high strengths with acceptable ductility. There are a variety of heat treatment temperatures and times so a range of properties can be obtained. A typical lamellar microstructure of Alpha 2 Orthorhombic is shown in Figure 83. The strength and ductility of an Orthorhombic alloy containing 25 at % niobium as a function of temperature are shown in Figures 84 a and b. The toughness of the Orthorhombic material also increases with test temperature or service temperature as shown in Figure 85. All of the different processing treatments shown in Figures 84 and 85 [32] result in a structure consisting of ordered Orthorhombic plates in an ordered β (B2 structure) matrix. The fine scale of the microstructure and the relative toughness of the Orthorhombic phase gives a good combination of strength and ductility in this class of material. Work continues on the Orthorhombic class of alloys but as of 1998 these alloys are considered promising but still not ready for introduction into real products.

### 4.5.2 Gamma Alloys (~50 at% Al)

The class of titanium intermetallics based on 50 at % Al is Gamma TiAl. Gamma is considered by many to be the most attractive Ti based intermetallic compound because of its low density, higher temperature capability and higher modulus. As in most situations, gamma also has the most restricted low temperature ductility and therefore poses the biggest challenge for introduction into real products. In fact, the ductility of Gamma is sufficiently low that it is very difficult to fabricate using traditional wrought processing methods (forging, rolling, etc.). Articles have been successfully fabricated by forging and sheet rolling has been demonstrated, but wrought processing of Gamma requires a level of care that suggests that making production quantities of components may not be practical, particularly from a cost standpoint. Fortunately, from an overall material application standpoint, investment casting of gamma appears to be relatively straightforward. Producing Gamma components by casting is more cost effective than wrought products at present. Further, casting technology for casting Gamma TiAl has matured rapidly over the last three or four years and now is essentially ready for production. The main barrier today is cost not the technological capability to produce cast components of sizes of up to ~20 kg pour weight. The cost of cast Gamma

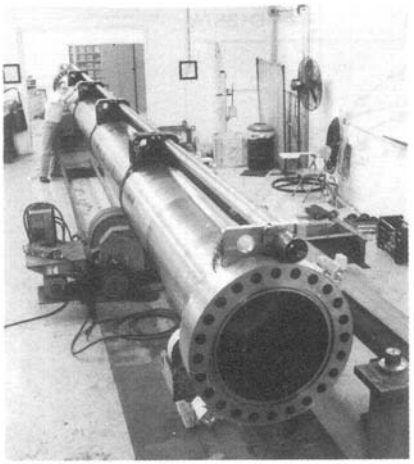

Fig. 81: Photos of heavy walled tubular drilling riser for a high pressure petroleum well (courtesey RMI Corp.).

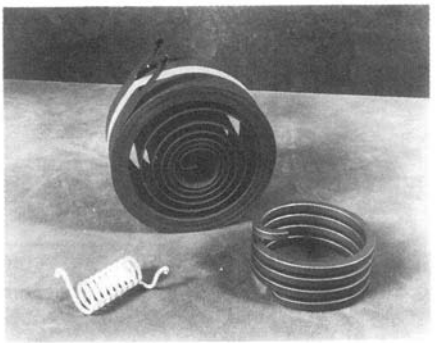

Fig. 82: Photo of Beta Ti-alloy springs (Ti-15-3, Beta C) used in Boeing aircrafts (courtesey Rod Boyer, Boeing).

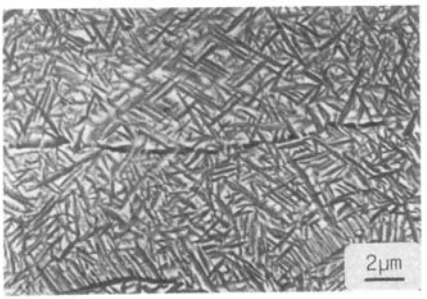


Fig. 83: Microstructure of beta solution treated and aged Ti-21Al-25Nb alloy.

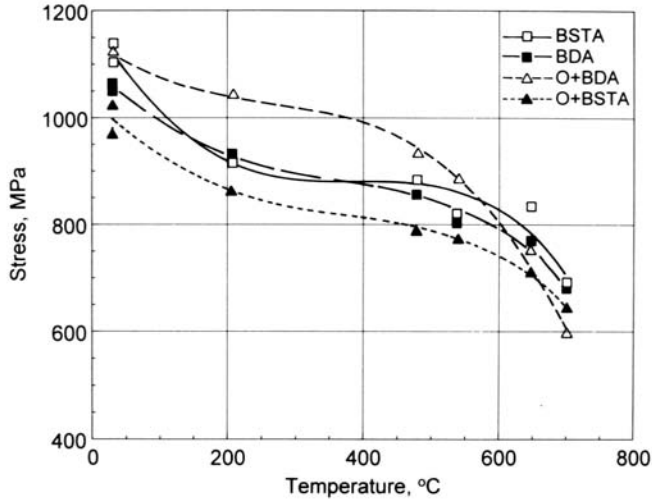


a) Yield strength

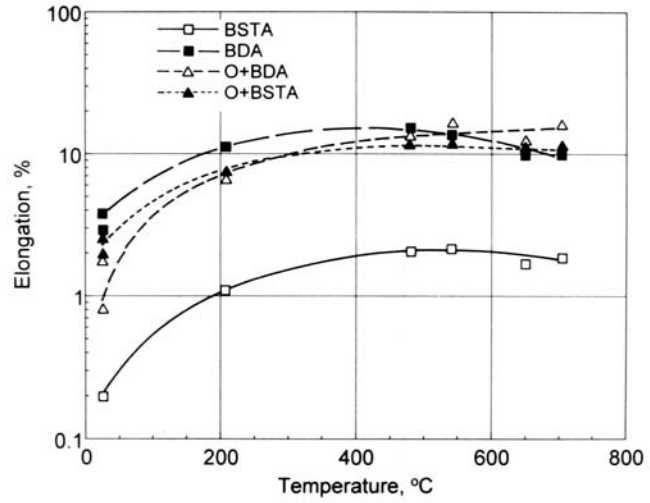


b) Tensile elongation

Fig. 84: Yield strength and ductility as a function of temperature for Orthorhombic Ti-21Al-25Nb alloy.

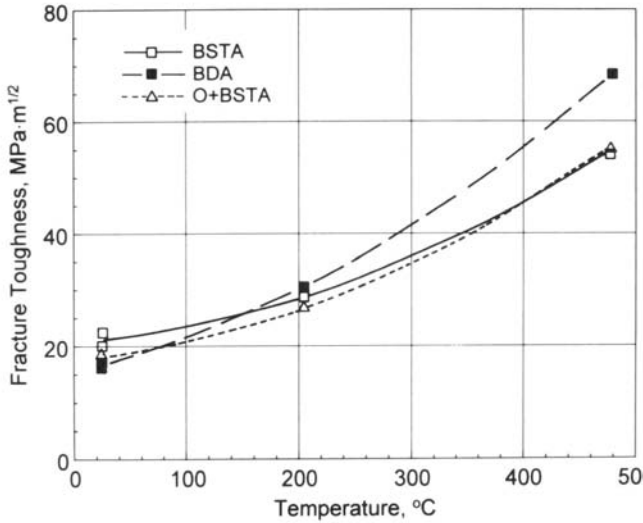


Fig. 85: Fracture toughness as a function of temperature for Orthorhombic Ti-21Al-25Nb alloy.

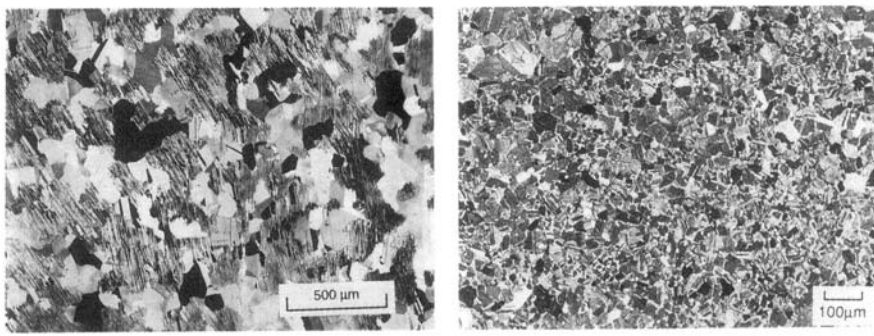


a) Cast (LM) b) Wrought (LM)

Fig. 86: Microstructure of Gamma Ti-48Al-2Cr-2Nb alloy.

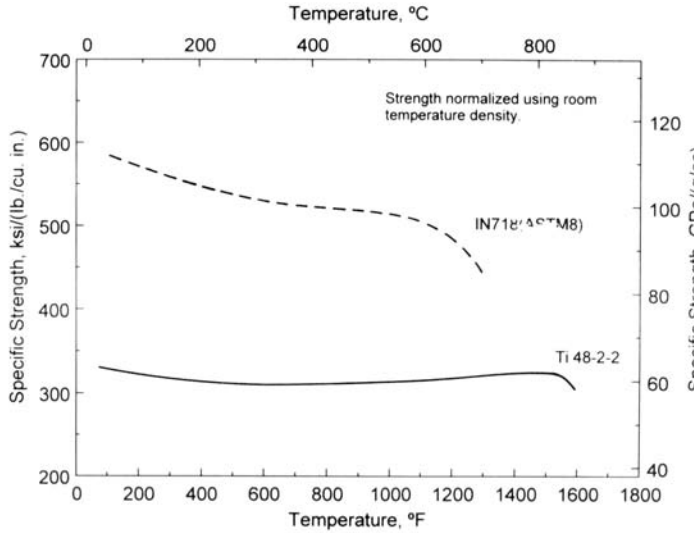


Fig. 87: Yield strength of Gamma Ti-48Al-2Cr-2Nb alloy and IN 718, normalized for density as a function of temperature.

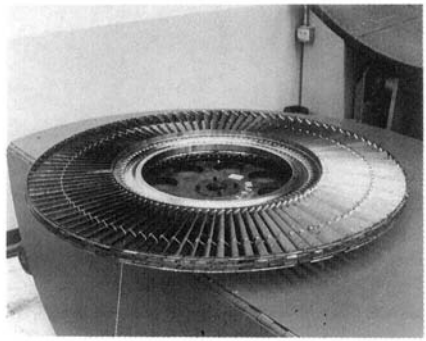

Fig. 88: Photo of low pressure turbine rotor containing cast Gamma (Ti-48Al-2Cr-2Nb) air foils.

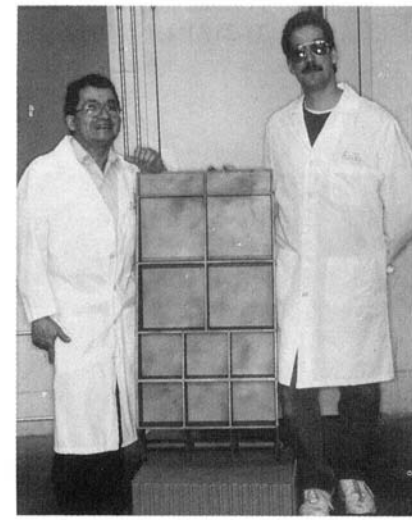

Fig. 89: Photo of a large Gamma (Ti-48Al-2Cr-2Nb) structural casting for an aero engine.

components are only marginally competitive at present, but will decrease over time as the casting technology further matures to give higher yields. These improved yields provided the basis to believe that cast Gamma will be affordable. Cost also will come down further as enough production applications emerge that there is a significant amount of scrap or revert available to reduce the cost of input material. The challenge today is to find some initial applications in order to get past the barrier of initial entry into service.

The properties of Gamma alloys depend significantly on microstructure. Gamma alloys can be processed and/or heat treated to have a bimodal microstructure with equiaxed primary gamma grains in a lamellar alpha-2 + gamma mixture or have a fully lamellar structure. The microstructures of both cast and of wrought Gamma Ti-48-2-2 are shown in Figures 86a and b. In terms of balancing tensile ductility, strength, and creep resistance, the preferred microstructure in Ti-48Al-2Cr-2Nb (Ti-48-2-2) is the bimodal gamma + lamellar structure. There are a number of alloy versions of Gamma being studied at different institutions and companies. The composition closest to commercial status may be the composition Ti-48-2-2. This alloy has been demonstrated to be quite castable and has about two percent room temperature ductility. Figures 87 a and b show the density normalized yield stress and ultimate strength of Ti-48-2-2 compared to the nickel base alloy IN718. The alloy Ti-48-2-2 has been extensively characterized in preparation for introduction into service. At this point it is accurate to say there appear to be no limiting characteristics that cannot be dealt with through thoughtful design. The principle barrier to production introduction of Ti-48-2-2 is cost, not performance. Today, investment cast Gamma components are more cost effective. This is because, as mentioned earlier, the casting technology for Gamma titanium aluminides has progressed remarkably in the last several years. There has been a successful factory engine test of a low pressure turbine rotor containing cast Gamma TiAl blades. Secondly large scale structural castings for potential introduction into the exhaust structure of large commercial engines has also been demonstrated. Photos of this rotor and of the large structural castings are shown in Figures 88 [33] and 89 [34].

There is also interest in cast Gamma for turbo-charger rotors for diesel engines and high performance automotive engines. These applications have also been demonstrated and the introduction will be paced by cost. Gamma is an attractive material for this application because of its high temperature capability and low density, the latter of which makes "spin up" time of a turbo-charger less and therefore the performance of a turbo-charged engines more attractive. Gamma also is an attractive material for exhaust valves in high performance internal combustion engines. The low mass of Gamma valves permits the use of lower spring forces which reduces weight and reduces valve train friction. Today, Gamma valves are too expensive for any but the highest performance engine applications. This may change over time as other markets develop for Gamma and the usage volume increases and the costs come down.

In summary, titanium based intermetallic compounds have been studied extensively and very intensively over the last ten years. Today, there are no production applications for these materials. This demonstrates the long time required to introduce a significantly

different material into real products. However, the attractiveness of these materials prevails and Gamma appears to be on track for limited production introduction in gas turbine engines as a replacement for nickel base superalloys. Use of these materials will permit significant weight reductions. The extent of use will be controlled by component cost. Thus a continued effort to achieve cost reductions and a concerted effort to find some initial production applications to gain economy of scale will be important to the long term outcome of this effort.

## 5. Titanium Production and Inspection

The intent of the previous Section 4 was to describe the physical metallurgy and application of titanium alloys. However, the success of many applications depends on the early stages of material production because this can have a large effect on the raw material quality. Raw material quality not only affects the the material properties, but also the reliability of components made from titanium alloys. Therefore, it is considered appropriate to include a very brief section on titanium production in order to impart some appreciation of this aspect of the overall titanium production and application spectrum.

There are a number of reliable treatises available on the production of raw, metallic titanium called sponge. The intent here is not reproduce these discussions but only to briefly summarize them for the purpose of providing a frame of reference. Pure metallic titanium used as the starting point for all titanium alloy production is obtained by reducing titanium tetrachloride ($TiCl_4$). $TiCl_4$ is made by chlorinating either Rutile ($TiO_2$) or Illmenite ($TiFeO_3$) to produce liquid $TiCl_4$. $TiCl_4$ is reacted with magnesium or sodium to form metallic titanium and magnesium chloride or sodium chloride. The process that uses magnesium is called the Kroll Process, while the one using sodium is called the Hunter Process. The chemical reactions which occur during reduction are described in detail in the articles mentioned earlier. The reduction process is a batch process performed at a high temperature in a closed reaction vessel (the reactor). After completion of the reaction, the reactor contains a solid cake (called a sponge cake) that is a mixture of magnesium or sodium chloride salts and metallic titanium. Some of the salt can be removed immediately but much of it is entrapped in the sponge cake. To remove the remaining salt, the sponge cake is removed from the reactor and mechanically crushed to permit access and removal of the remaining chlorides. The chlorides are removed by leaching with acid or through a vacuum distillation process. The latter process is done by heating the sponge granules in a high temperature retort under vacuum to cause the chlorides to volatilize. Environmental concerns about disposal of the leaching waste stream have made vacuum distillation the preferred method in recent years. In either case the resulting metallic Ti has the form of porous granules, hence the name sponge. For specific applications, where very high purity is required, the sponge can then be subsequently electro-refined by an electrolytic process. Electro-refined titanium is now used in substantial quantities as sputtering targets during the fabrication of micro-electronic devices. In these applications, very high purity titanium is required

to avoid introduction of unwanted chemical species that could affect the semiconductor behavior.

The sponge made by the process outlined in a very brief way above becomes the raw input material for the initial melting of titanium alloys. During vacuum distillation there is some unavoidable sintering of the sponge. The vacuum distilled sponge is sheared or crushed to produce a granular product in which the maximum desired particle size is typically somewhere between 1 and 2 centimeters in diameter, depending on the alloy and the grade of Ti being melted. The sponge is then mixed in appropriate portions with alloying elements in particulate form. These are either pure elemental powders or particles of master alloys which contain two or more of the desired chemical constituents. The mixture of alloying elements and sponge is blended mechanically , e.g. in a twin cone blender. It then is mechanically compacted using a screw or hydraulic press to form briquettes for a first melt electrode. These briquettes are welded together in a dry box using a plasma torch to form the first melt electrode. Melting of titanium is a crucial step in producing a high quality, homogeneous alloy product. Because of the reactivity of molten titanium with oxygen and nitrogen, it must always be melted under vacuum and the most common method is vacuum arc melting and remelting. Even after acid leaching or vacuum distillation the sponge has a very high surface area and therefore still contains modest quantities of chloride adsorbed to the sponge surface. Therefore, gas evolution during the first melt is substantial and vacuum arc melting furnace with very high capacity pumping systems are required. Arc melting is accomplished by initiating an electric arc between some Ti placed in the bottom of the water cooled copper crucible of the arc melting furnace. The molten Ti drips from the first melt electrode to form a pool that eventually fills the water cooled copper mold to form a primary melt ingot. At any one time, the volume of the molten pool is a small fraction of the total ingot weight. This helps minimize short range freezing segregation but also limits large scale homogenization of alloy chemistry.

Current commercial Ti alloy production technology, except for alloys very prone to chemical segregation, allows production of ingots that are between 75 and 90 centimeters in diameter. These ingots can weigh as much as 5,000 kg. For structural applications this primary ingot is vacuum arc remelted (VAR) a second time in order to improve the ingot soundness and the chemical homogeneity. After this, it is soaked in a high temperature furnace for tens of hours to permit diffusional homogenization. It is then forged into a primary starting stock to be subsequently converted to billet, bar, plate, or sheet. For very high performance applications, such as rotating parts in jet engines, the material is typically remelted twice and the product is known as triple melt or premium quality rotor grade material. The third melt further improves the chemical homogeneity and achieves some additional refining to remove or minimize the presence of melt related defects which will be mentioned later.

A new melting technology, which is gaining acceptance, is called cold hearth melting (CHM). Cold hearth melting is done as a skull melting operation using a water cooled copper hearth in either an electron beam or plasma arc furnace. The CHM process is

used as the penultimate melting step for high performance applications and replaces the second VAR process in the triple melt process. Hearth melting is important because it appears to give a higher purity and a higher quality product, although the quality of triple melt VAR material also has improved substantially in the last several years. Premium quality rotor grade CHM material thus is melted in the following sequence: VAR + CHM + VAR.

There are two types of melt related defects that can be present in Ti alloys. These occur infrequently, but when present have a serious effect on the properties, especially fatigue life. One of these is the presence of nitrogen or other interstitial element stabilized regions called Type 1 or Hard Alpha defects. As discussed in the phase equilibrium section of this chapter titanium has a strong propensity to react with oxygen, nitrogen, and carbon and the reaction products are stable, high melting point compounds. The most common of these is Ti Nitride (TiN). During the melting process if, for example, there is an air leak in the vacuum system and air is admitted to the VAR or CHM furnace chamber, a chemical reaction can occur to form titanium nitride. Titanium nitride has both a very high melting temperature and a relatively high density. It is also very hard and extremely brittle. The presence of TiN in highly stressed Ti alloy components has very deleterious effects on properties, particularly low cycle fatigue. Once formed, titanium nitride or Hard Alpha, as its often called is very difficult to remove from the material. Refining these inclusion out by dissolving them in molten titanium is possible but the kinetics are relatively slow, making this an uneconomical process. The cold hearth melting process allows a more sustained exposure of the material in the molten state permits improved refining and increases the possibility for dissolving small titanium nitride particles. Experience has shown that even hearth melting cannot remove large titanium nitride particles. Thus today the preferred approach for making so-called premium quality rotor grade titanium is to exert stringent control over the input materials, the initial VAR practice, and the subsequent melt practice whether it is two more VAR melts or CHM + VAR.

The presence of Hard Alpha (also known as Type 1 Defects) in a rotating gas turbine engine part leads to very early crack initiation because its hard, brittle nature causes it to crack early in the component service history. This has severe consequences with regard to the fatigue life of the component. Therefore, it is essential that every caution be taken to minimize the possibility of existence of Hard Alpha in a final product. The second melt related defect is called Soft Alpha (also known as a Type-2 defect) and results from variations in chemical composition especially aluminum. Once present, aluminum rich regions in titanium alloys are very difficult to subsequently remove, at least without substantial impact on the ability to create the desired microstructure in the final product. As mentioned also in the phase equilibrium section high aluminum leads to the formation of alpha 2 and therefore the aluminum rich regions are deleterious to low cycle fatigue performance. Type 2 melt related defects are much less serious but nevertheless need to be avoided for premium quality rotor grade materials. A third type of melt-related defect is the segregation (local enrichment) of beta stabilizing elements during ingot

solidification. These regions lead to local depression of the beta transus temperature, which leads to regions that contain less or no primary alpha phase. These regions are called "beta flecks" and have adverse affects on the fatigue crack initiation behavior of the material.

One of the key aspects of producing high quality titanium billets for rotating parts for aircraft engines is to have very sensitive inspection capability of the billet before it is made into forgings. Billet is an intermediate Ti mill product shaped like an axi-symmetric cylinder. Billet is produced by initially forging the ingot to smaller dimensions and often finishing in a rotary machine (sometimes called a GFM). Over the years, titanium producers have learned how to ultrasonically inspect their product to increasingly sensitive levels. Today it is possible to inspect a 9" billet to a number one flat bottom hole ultrasonic standard. (A number one flat bottom hole is less than a half millimeter in diameter.) Such sensitive sonic inspection allows most melt related defects, both Type 1 and Type 2 to be detected during the inspection process which occurs before the product is shipped to a forger. Ultrasonic inspection of titanium alloys is a complicated subject for a variety of reasons including the elastic anisotropy of the alpha phase which leads to noise and the high attenuation characteristics of the beta phase. The reader interested in this subject should read one of several treatises on this subject also as can be found in the references.

This brief summary of titanium production and inspection is not intended to provide any substantial knowledge of the subject but rather to alert and sensitize the reader to the importance of the production aspects of titanium technology and the interaction between production methods and product performance.

## References

1. The Science, Technology and Application of Titanium, R. I. Jaffee and N. E. Promisel, Eds., Pergamon Press, Oxford, UK, 1970.
2. Titanium Science and Technology, R. I. Jaffee and H. M. Burk, Eds., Plenum Press, New York, USA, 1973.
3. Titanium and Titanium Alloys, J. C. Williams and A. F. Belov, Eds., Plenum Press, New York, USA, 1982.
4. Titanium '80, Science and Technology, H. Kimura and O. Izumi, Eds., AIME, New York, USA, 1980.
5. Titanium, Science and Technology, G. Lütjering, U. Zwicker and W. Bunk, Eds., DGM, Oberursel, Germany, 1985.
6. Sixth World Conference on Titanium, P. Lacombe, R. Tricot and G. Beranger, Eds., Les Editions de Physique, Les Ulis, France, 1988.
7. Titanium '92, Science and Technology, F. H. Froes and I. L. Caplan, Eds., TMS, Warrendale, USA, 1993.
8. Titanium '95, Science and Technology, P. A. Blenkinsop, W. J. Evans and H. M. Flower, Eds., The University Press, Cambridge, UK, 1996.
9. A. Zarkades and F.R. Larson, The Science, Technology and Application of

Titanium, Pergamon Press, Oxford (1970) 933.
10. H. Conrad, M. Doner and B. de Meester, Titanium Science and Technology, Plenum Press, New York (1973) 969.
11. R. Boyer, G. Welsch, E. W. Collings (Eds.), Materials Properties Handbook: Titanium Alloys, ASM International, Metals Park (1994).
12. P.G. Partridge, Met. Rev., 12 (1967) 169.
13. M. H. Yoo, Met. Trans., 12A (1981) 409.
14. N. E. Paton, J. C. Williams and G. P. Rauscher, Titanium Science and Technology, Plenum Press, New York (1973) 1049.
15. I. P. Jones and W. B. Hutchinson, Acta Met., 29 (1981) 951.
16. N. E. Paton, R. G. Baggerly and J. C. Williams, Rockwell Report (1976).
17. N. E. Paton and J. C. Williams, 2nd Int. Conf. Strength of Metals and Alloys, ASM, Metals Park (1970) 108.
18. ASM Handbook Vol. 3, Alloy Phase Diagrams, ASM International, Metals Park (1992).
19. W. G. Burgers, Physica, 1 (1934) 561.
20. J. B. Newkirk and A. H. Geisler, Acta Met., 1 (1953) 370.
21. J. C. Williams, B. S. Hickman and D. H. Leslie, Met. Trans. 2 (1971) 477.
22. D. de Fontaine, Acta Met., 18 (1970) 275.
23. A. Gysler, G. Lütjering and V. Gerold, Acta Met., 22 (1974) 901.
24. Z. Liu and G. Welsch, Met. Trans., 19A (1988) 1121.
25. J. L. Smialek et al., Mat. Res. Soc. Symp. Proc., Vol. 364 (1995) 1273.
26. J. O. Peters, G. Lütjering, M. Koren, H. Puschnik and R. R. Boyer, Titanium '95, The University Press, Campbridge, UK (1996) 1403.
27. G. Lütjering and A. Gysler, Titanium Science and Technology, DGM, Oberursel, Germany (1984) 2065.
28. G. Lütjering, A. Gysler and L. Wagner, Sixth World Conference on Titanium, les editions de physique, Les Ulis, France (1988) 71.
29. G. Wegmann, G. Lütjering, J. Albrecht, K.-D. Folkers and C. Liesner, Titanium '95, The University Press, Cambridge, UK (1996) 895.
30. G. Terlinde and G. Fischer, Titanium '95, The University Press, Cambridge, UK (1996) 2177.
31. H. M. Flower, P. R. Swann and D. R. F. West, Met. Trans. 2 (1971) 3289.
32. A. P. Woodfield and B. H. Lawless, Metallic Materials for Lightweight Applications, Proceedings of the Sagamore Army Materials Research Conference (1993) 89.
33. C. M. Austin and T. J. Kelly, Superalloys 1996, TMS, Warrendale (1996) 539.
34. P. Bartolotta, J. Barrett, T. J. Kelly and R. Smashey, J. of Metals, May 1997.

**Problems**

1. The α+β alloy Ti-6Al-4V will be applied for a fatigue critical part with a bi-modal microstructure, consisting of equiaxed primary α in a transformed β matrix, both having grain dimensions of 15μm. The starting material was hot rolled in the β phase field and water quenched. The annealing temperature of 950°C results in equal volume fractions of equiaxed primary α and β phases. Estimate the miminum homogenization time at 950°C to reach approximately the necessary concentration of the respective alloying elements in the α phase and in the β phase (Hint: Use the equation $x = \sqrt{D \cdot t}$).

2. The blades of a Near-α Ti-alloy in an aircraft engine compressor experience a constant centrifugal stress along the blade axis of 150 MPa at a temperature of 525°C. The blade length is 25 mm and the gap between the blade tips and the casing is 0.75 mm at room temperature. Creep tests of this alloy at the operating conditions showed a plastic creep strain of 0.1% after 100 h, followed by a steady-state creep rate of $5 \cdot 10^{-10}$ $s^{-1}$. Predict the safe lifetime for these blades by considering also the thermal expansion (Table 4) and the elastic strain (E = 85 GPa) for this application.

3. During the design phase of a new airplane, a serious weight problem arises. You are responsible for a heavy forging to be made from a high strength 7XXX Aluminum-Alloy (weight: 100 kg, thickness: 65mm). The critical design property is the HCF ($10^7$ cycles) fatigue strength (R = -1), which is 180 MPa for the 7XXX alloy. The safety factor allows only 75% of the HCF strength to be taken as the maximum stress amplitude. Would you recommend a change in material to Titanium alloys (α+β or β) if the saving in the total operating cost is $ 200/kg? (Remark: Changes in weight and stress can be made only by changes in thickness of the forging).

For your decision, the following values are given:

<u>7XXX alloy</u>
E: 70 GPa, ρ (density): 2.80 g/cm$^3$, price: $ 12/kg.

<u>α+β alloy</u> (select Ti-6Al-4V)
E (see Table 10), ρ (take α-Ti value from Table 4), HCF strength (take best value for bi-lamellar in Fig. 54), price: $ 55/kg.

<u>β alloy</u> (select β-CEZ)
E (see Table 11), ρ (take β-Ti value from Table 4), HCF strength (take best value from Fig. 59), price: $ 70/kg.

a) Unfortunately, in case of changing the material the maximum elastic strain can be increased only by 20% over that of the 7xxx forging. Which alloy would you choose and how much money would you save?

b) In case of not having the limitation in the maximum allowable elastic strain, which alloy would you choose and how much money would you save?

4. For a structural aerospace part (material: Ti-6242) you calculated the number of cycles to fracture ($N_F = 3.7 \times 10^7$ cycles) assuming an initial crack size of $a_i = 25\mu m$ and taking the macrocrack propagation curve (AC) shown in Fig. 40. For that calculation you used the following equations and informations:

$R = 0.1$, $\Delta\sigma = 400$ MPa, $K_{Ic}$ (see Table 9), $K = 1.244\,\sigma\sqrt{a}$, $da/dN = C \cdot \Delta K^n$.

What would be the number of cycles to fracture ($N_F$), if you would have made the correct choice and would have taken the microcrack propagation curve (AC) in Fig. 40 instead of the macrocrack propagation curve? (Hint: Avoid $n = 2.0$, take $n = 2.1$).

5. Learning from the solution of problem 4, you will be able to make the correct choice for the optimum microstructure (bi-modal or lamellar) of the IMI 834 alloy to be taken for a fatigue critical part in the compressor section of an aero engine. For your calculation of $N_F$, you need the following values and equations:

$R = 0.1$, $\Delta\sigma = 180$ MPa, initial crack size: 25μm, $K = 1.244\,\sigma\sqrt{a}$, $da/dN = C \cdot \Delta K^n$, $K_{Ic}$ of bi-modal microstructure: see Table 9, $K_{Ic}$ of lamellar microstructure: 65 MPa $m^{1/2}$, for da/dN-ΔK curves: see Fig. 47.

Which microstructure would you take?

6. You have been given the task of designing a simple flat spring. The spring with a rectangular cross-section (width w, thickness t) must be 1.22m long and deflect 2.54cm under a 22.24 KN load applied at the center of the 1.22m span. You have two materials to select from, steel or beta-titanium. The spring cannot exceed the yield strength of the material. Which is the best material choice based on lightest weight and give that weight? What is the best choice if low cost is critical, and give that cost?

| | β-Titanium | Steel |
|---|---|---|
| Yield Strength, Y | 1207 MPa | 1517 MPa |
| Young's Modulus, E | 100 GPa | 207 GPa |
| Density, ρ | 4.5 g/cm$^3$ | 7.9 g/cm$^3$ |
| Cost, $/kg | $50/kg | $2.20/kg |

$\sigma_{max} = MC/I$ $\quad C = t/2$ $\quad M = (Pxl)/2$ $\quad I = wt^3/12$ $\quad \delta = Pl^3/48EI$

7. You must select a material for a pressure vessel. You can choose between an α+β Titanium alloy (Ti-6Al-4V ELI, coarse lamellar microstructure) and a high strength β

Titanium alloy. In addition to the selection of the alloy you must calculate the thickness of the wall to be used. The tank wall must be as thin as possible for minimum weight. For safety reasons any crack which forms must be capable of growing through the tank wall forming a leak which will vent the pressure thus avoiding an explosion. The cylindrical tank has an inside diameter of 30cm and a length of 1.52m. Which alloy would you select and what is the minimum wall thickness, t, of the tank wall ? What is the stress in the lightest tank at a maximum pressure of 20.7 MPa?

| | $\alpha+\beta$ Titanium | $\beta$ Titanium |
|---|---|---|
| Ultimate Strength, UTS | 827 MPa | 1379 MPa |
| Fracture toughness, $K_{Ic}$ | 88 MPa$\sqrt{m}$ | 55 MPa$\sqrt{m}$ |

$\sigma$ = Pressure · Diameter/2t

Stress Intensity for a half-penny shaped part through crack with a crack depth a: $K_{Ic} = 0.71\ \sigma\sqrt{\pi a}$

Stress Intensity for a through crack with a crack length in axial direction of 2 a: $K_{Ic} = 1.12\ \sigma\sqrt{\pi a}$